NJC

PAPER

Cite this: *New J. Chem.*, 2016, **40**, 5861

Effects of N,N-heterocyclic ligands on the *in vitro* cytotoxicity and DNA interactions of copper(II) chloride complexes from amidino-*O*-methylurea ligands†

Atittaya Meenongwa,[a] Rosa F. Brissos,[b] Chaiyaporn Soikum,[c] Prapansak Chaveerach,[c] Patrick Gamez,[bd] Yanee Trongpanich[e] and Unchulee Chaveerach*[a]

Received (in Montpellier, France) 4th December 2015, Accepted 19th April 2016

DOI: 10.1039/c5nj03439f

www.rsc.org/njc

Copper(II) complexes based on guanidine derivatives have been synthesized by the addition of N,N-heterocyclic ligands, yielding four new compounds, $[Cu(L^1)(bipy)]Cl_2$ (**1**), $[Cu(L^1)(phen)]Cl_2$ (**2**), $[Cu(L^2)(bipy)Cl_2]$ (**3**) and $[Cu(L^2)(phen)]Cl_2$ (**4**) (L^1 = amidino-*O*-methylurea, L^2 = *N*-(benzyl)-amidino-*O*-methylurea, bipy = 2,2′-bipyridine and phen = 1,10-phenanthroline), and their biological activities have been studied. All complexes were characterized by elemental analysis and various spectroscopic methods (FT-IR, mass, diffuse reflectance, UV-Vis and EPR). Their structures were proposed to be square planar (for **1**, **2** and **4**) and distorted octahedral (for **3**). Their interactions with calf thymus (CT) DNA were examined by electronic absorption titration, viscosity measurements, circular dichroism spectroscopy, DNA-melting analysis, fluorescence spectroscopy and determination of the stoichiometry. Two possible DNA-binding modes of the complexes are proposed to be non-intercalation at low [complex]/[DNA] ratios and intercalation at high [complex]/[DNA] ratios. Their nuclease activities, investigated by gel-electrophoresis and atomic-force microscopy (AFM), show that the complexes can cleave plasmid pBR322 DNA, probably through oxidative pathways. Moreover, their *in vitro* cytotoxic activities against three human tumor cell lines (small cell lung carcinoma (NCI-H187), oral cavity carcinoma (KB) and breast adenocarcinoma (MCF-7)) and their antibacterial activities toward three Gram negative bacteria (*E. coli*, *Salmonella* and *Campylobacter*) were determined. The complexes in this system exhibit a more potent anticancer effect against the NCI-H187 cell line. Complex **2** had the best inhibition efficiency, particularly against *Campylobacter*. Indeed, the biological activities of the complexes follow the trend of **2** > **4** > **1** > **3**.

1. Introduction

The mechanisms of the interaction of DNA with inorganic compounds have been intensely investigated. This valuable information is of paramount importance in developing metal-based drugs. A square planar platinum complex, $[Pt(NH_3)_2Cl_2]$ or cisplatin, the first generation anticancer drug,[1] shows high cytotoxicity to several types of cancers, such as testicular, ovarian, head and neck and cell lung cancers,[2] by coordination with DNA; this interaction interferes with mitosis, causing the cancer cell to undergo apoptosis.[3] However, cisplatin has several side effects, which has encouraged many researchers to develop new metal-based anticancer drugs with higher curative potential, lower toxicities and target-specific properties.

Copper is recognized as a bio-essential trace element in the human body due to the enzymatic functions arising from its oxidative nature.[4] In addition, copper is inexpensive and can form complexes with various coordination geometries. Some copper(II) complexes with organic ligands are reported to be effective DNA-binding and cleaving agents as well as being active against bacteria and cancer cells.[5–7] Consequently, copper is suitable as an alternative element, providing benefits in both the design and various applications of metal complexes.

In our previous studies, we intensively investigated the biological behaviors of a series of copper(II) complexes containing

[a] *Materials Chemistry Research Center, Department of Chemistry and Center of Excellence for Innovation in Chemistry, Faculty of Science, Khon Kaen University, Khon Kaen 40002, Thailand. E-mail: sunchul@kku.ac.th*
[b] *Departament de Química Inorgànica, Universitat de Barcelona, Martí I Franqués 1-11, 08028 Barcelona, Spain*
[c] *Department of Veterinary Public Health, Faculty of Veterinary Medicine, Khon Kaen University, Khon Kaen 40002, Thailand*
[d] *Institució Catalana de Recerca i Estudis Avançats (ICREA), Passeig Lluís Companys, 23, 08010 Barcelona, Spain*
[e] *Department of Biochemistry, Faculty of Science, Khon Kaen University, Khon Kaen 40002, Thailand*

† Electronic supplementary information (ESI) available. See DOI: 10.1039/c5nj03439f

bidentate amidino-*O*-methylurea (L^1) and *N*-(benzyl)-amidino-*O*-methylurea (L^2). These ligand systems have versatile hydrogen-bonding potential,[8,9] which may be the reason for the biological activities of the copper(II) complexes. Two monomeric copper(II) compounds, $[Cu(L^1)_2Cl_2]$ and $[Cu(L^2)_2Cl_2]$, with square planar geometry,[9] display DNA-binding capabilities through non-intercalative modes, DNA-cleaving ability *via* oxidative processes and antibacterial activity toward *Campylobacter*.[10] Recently, two dimeric compounds of these ligands, $[Cu(L^1)Cl_2]_2$ and $[Cu(L^2)Cl_2]_2$, whose structures were proposed to have an approximate square-pyramidal geometry,[11] exhibited DNA-binding and cleaving properties as well as antibacterial activity against three human-food poisoning bacteria, including *Salmonella*, *E. coli* and *Campylobacter*; they also exhibited anticancer activity toward small cell lung carcinoma and epidermoid carcinoma of the oral cavity.[12]

In this work, the biological properties of copper(II) complexes based on the dimeric compounds $[Cu(L^1)Cl_2]_2$ and $[Cu(L^2)Cl_2]_2$ have been improved by the addition of N,N-heterocyclic ligands. 2,2′-Bipyridine (bipy) and 1,10-phenanthroline (phen) were selected as the second ligands. Some copper(II) complexes containing bipy or phen have shown DNA-binding and DNA cleavage properties.[6,13–15] Herein, we report the synthesis and characterization of four copper(II) complexes, including $[Cu(L^1)(bipy)]Cl_2$ (**1**), $[Cu(L^1)(phen)]Cl_2$ (**2**), $[Cu(L^2)(bipy)Cl_2]$ (**3**) and $[Cu(L^2)(phen)]Cl_2$ (**4**). To investigate the potential DNA-binding properties of the complexes toward calf thymus (CT) DNA, several methods, including electronic absorption titration, viscosity measurements, circular dichroism (CD) spectroscopy, thermal denaturation, fluorescence spectroscopy and determination of stoichiometry, were employed. The effective cleavage of pBR322 plasmid DNA by the complexes was further examined by gel electrophoresis and atomic-force microscopy (AFM). Their cytotoxicity against three human cancer cell lines (*i.e.* small cell lung carcinoma (NCI-H187), epidermoid carcinoma of the oral cavity (KB) and breast adenocarcinoma (MCF-7)) was determined using the resazurin microplate assay (REMA). Furthermore, all complexes were screened for their antibacterial activity against a series of human food-poisoning bacterial species (*Salmonella*, *E. coli* and *Campylobacter*) by the agar-well diffusion method.

2. Experimental

2.1. Materials and instruments

2,2′-Bipyridine (bipy) and 1,10-phenanthroline monohydrate (phen) were obtained from Acros Organics and Carlo Erba, respectively. All other chemicals and solvents (analytical grade) were commercially available and were used without further purification. DNA sodium salt from calf thymus (CT-DNA, Type I fibrous) was purchased from Sigma-Aldrich. Plasmid pBR322 DNA (4361 bp, 0.25 μg μL^{-1}) was obtained from Bio Basic INC and Roche Farma, S.A. Tris(hydroxymethyl) aminomethane (Tris base) and ethidium bromide (EB) solution (10 mg mL^{-1}) were purchased from Promega. Agarose (D-1, low EEO) was purchased from Pronadisa. *N*-(2-Hydroxyethyl)piperazine-*N*′-(2-ethanesulfonic acid) (HEPES) was obtained from Sigma-Aldrich. All reagents involved in the DNA experiments were of molecular biology grade and were used as received. Doubly distilled water was used to prepare the buffer solution (3% MeOH in Tris-buffer containing 5 mM Tris-HCl and 50 mM NaCl, pH = 7.2).

Elemental analyses (C, H and N) were determined using a Perkin-Elmer PE-2400II CHNS/O elemental analyzer. Infrared spectra were recorded in the range of 400 to 4000 cm^{-1} using KBr pellets on a Perkin-Elmer Spectrum One FT-IR spectrophotometer. Electrospray ionization (ESI+) mass spectra in MeOH were recorded on a Bruker micrOTOF mass spectrometer. Diffuse reflectance spectra were collected on a Shimadzu 3101 UV-Vis-NIR scanning spectrophotometer. Electronic absorption spectra of sample solutions in MeOH and DMSO were recorded on an Agilent 8453 UV-Vis spectrophotometer using cuvettes of 1 cm path length. Electron spin resonance spectra in frozen DMSO solution at 77 K were detected by a RE-2X electron spin resonance spectrometer operating at ν = 9.16 GHz (X-band). Fluorescence measurements were analyzed with a Shimadzu RF-5301PC spectrofluorophotometer. Circular dichroism (CD) spectra were recorded on a Jasco J-815 spectropolarimeter (this service was provided by the Research Instrument Center, Khon Kaen University, Thailand). The amount of copper for each stoichiometric ratio was determined with a Perkin-Elmer AAnalyst 100 atomic absorption spectrophotometer. The electrophoretic band intensities were visualized with a Bio-Rad Gel Doc 2000 system using LABWORK software. The atomic-force microscopy (AFM) images were obtained by a Nanoscope V Multimode 8 AFM (Bruker AXS) operating in the PEAK FORCE tapping mode. A commercial Si-tip on nitride lever cantilevers (SNL, Bruker) with a force constant of 0.4 N m^{-1} was used.

2.2. Complex preparation

2.2.1. Copper(II) complexes of amidino-*O*-methylurea and its derivative. The two dimeric copper(II) complexes, $[Cu(L^1)Cl_2]_2$ and $[Cu(L^2)Cl_2]_2$ were prepared according to our published procedure[16] and were used as the starting complexes.

2.2.2. Copper(II) complexes with N,N-heterocyclic ligands. A methanolic solution (25 mL) of 2,2′-bipyridine (0.1562 g, 1 mmol) or 1,10-phenanthroline monohydrate (0.1980 g, 1 mmol) was added dropwise to a methanolic solution (25 mL) of $[Cu(L^1)Cl_2]_2$ (0.2505 g, 0.5 mmol) or $[Cu(L^2)Cl_2]_2$ (0.3405 g, 0.5 mmol) under stirring at ambient temperature, and the pH was subsequently adjusted to 7 using NaOH. The reaction mixture was stirred for 2 h and then filtered. The volume of the filtrate was reduced by 50% and the remaining filtrate underwent slow evaporation. A purple or pink product was acquired and was further recrystallized in ethanol.

*$[Cu(L^1)(bipy)]Cl_2$ (**1**).* Purple solid. Yield, 0.3486 g, 85.8%. Anal. calc. for $C_{13}H_{16}CuN_6OCl_2$ (MW. 406.50) (%): C, 38.38; H, 3.94; N, 20.66. Found: C, 37.69; H, 4.04; N, 20.63. Melting point (°C): 127.5–128.4. FT-IR (KBr, cm^{-1}): 3429s, 3323s, 1613m, 1583s, 1528m, 1498m, 1474m, 1448m, 1405m, 1317w, 1282w, 1223w, 1193w, 1137w, 1095w, 1071w, 1032w, 1019w, 966w, 771w, 729w, 683w, 635w, 534w, 414w. Solubility: highly soluble in polar solvents such as water, MeOH and DMSO.

*[Cu(L^1)(phen)]Cl$_2$ (**2**).* Purple solid. Yield, 0.3136 g, 72.8%. Anal. calc. for $C_{15}H_{16}CuN_6OCl_2$ (MW. 430.7) (%): C, 41.79; H, 3.71; N, 19.50. Found: C, 41.45; H, 3.91; N, 19.39. Melting point (°C): 171.7–172.3. FT-IR (KBr, cm^{-1}): 3486s, 3394s, 3322s, 3208s, 3060m, 1643s, 1574s, 1523s, 1494s, 1469s, 1428m, 1393m, 1347w, 1289w, 1224m, 1190m, 1149w, 1099m, 1007w, 927w, 872w, 851m, 780w, 735w, 722m, 645w, 574w, 521w. Solubility: highly soluble in polar solvents such as water, MeOH and DMSO.

*[Cu(L^2)(bipy)Cl$_2$] (**3**).* Pink solid. Yield, 0.1876 g, 37.8%. Anal. calc. for $C_{20}H_{22}CuN_6OCl_2$ (MW. 496.5) (%): C, 48.32; H, 4.43; N, 16.91. Found: C, 48.44; H, 4.59; N, 17.06. Melting point (°C): 180.0–181.3. FT-IR (KBr, cm^{-1}): 3369m, 3332m, 2951w, 2923w, 1589s, 1495s, 1472s, 1451s, 1414s, 1394s, 1357m, 1323w, 1262m, 1219w, 1199w, 1189w, 1122w, 1090w, 1067w, 1026w, 1001w, 934w, 756m, 708m, 594w, 580w. Solubility: highly soluble in MeOH and DMSO but insoluble in water.

*[Cu(L^2)(phen)]Cl$_2$ (**4**).* Purple solid. Yield, 0.4384 g, 84.2%. Anal. calc. for $C_{22}H_{22}CuN_6OCl_2$ (MW. 520.7) (%): C, 50.70; H, 4.23; N, 16.13. Found: C, 50.79; H, 4.14; N, 15.65. Melting point (°C): 189.0–190.4. FT-IR (KBr, cm^{-1}): 3434m, 3265m, 3123w, 3062w, 1605s, 1524s, 1495m, 1473s, 1427m, 1347w, 1277w, 1250w, 1221w, 1200w, 1186w, 1141w, 1126w, 1090w, 1042w, 928w, 906w, 853w, 758w, 719m, 580w. Solubility: highly soluble in MeOH and DMSO but insoluble in water.

2.3. DNA binding experiments

To circumvent some problems caused by organic solvents, Tris-buffer (5 mM Tris-HCl/50 mM NaCl, pH = 7.2) containing 3% MeOH was selected for use in all experiments with CT-DNA and copper(II) complexes. The DNA stock solution prepared in this buffer gave a UV-absorbance ratio A_{260}/A_{280} of about 1.8 to 1.9 (where A_{260} and A_{280} are the absorbances of a DNA sample at 260 and 280 nm, respectively), indicating that DNA was sufficiently free of protein contamination.[17] The stock solution was maintained at 4 °C and was used within 4 days. A 10-fold dilution of DNA concentration was determined spectrophotometrically at 260 nm using the molar extinction coefficient value of 6600 M^{-1} cm^{-1}.[18] The stock solutions of both DNA and the copper(II) complexes were freshly prepared before use.

2.3.1. Electronic absorption titration. Absorption titration experiments were carried out with a constant concentration of copper(II) complexes, *viz.* 10 μM, and varying concentrations of CT-DNA (2 to 15 μM) in 3% MeOH/Tris-buffer at pH 7.2. The complex and DNA solutions were incubated at 37 °C for 24 h. Subsequently, the spectra were recorded with a UV-Vis spectrophotometer at ambient temperature. To subtract the absorption due to DNA itself (in each sample), the spectra of free CT-DNA (namely, in the absence of copper compounds) were recorded at the same concentrations of 2 to 15 μM and were used as blanks. To compare the DNA-binding strengths of the four compounds, their intrinsic binding constants (K_b) were calculated from the plots of [DNA]/($\varepsilon_a - \varepsilon_f$) *vs.* [DNA] using eqn (1); K_b is given by the ratio of the slope to the y intercept.[19]

$$[DNA]/(\varepsilon_a - \varepsilon_f) = [DNA]/(\varepsilon_b - \varepsilon_f) + 1/K_b(\varepsilon_b - \varepsilon_f) \quad (1)$$

where [DNA] is the concentration of DNA, ε_a is given by A_{obsd}/[Cu], ε_f is the extinction coefficient for the free metal complex and ε_b is the extinction coefficient for the metal complex in the fully bound form.

2.3.2. Viscometric titration. Viscosity experiments were carried out with an Ubbelodhe viscometer, immersed in a water bath at 37 ± 0.1 °C. The viscosity of a 200 μM solution of CT-DNA was determined in the presence of the complexes using different [complex]/[DNA] ratios in the range of 0.00 to 2.00 with 0.20 intervals. The flow time for each sample was recorded in triplicate with a digital stopwatch and then averaged. The relative viscosity (η) was determined from the flow time of the DNA-containing solutions (t) corrected by the flow time of the free buffer (t_0): $\eta = (t - t_0)/t_0$.[20] The data are presented as the plot of the relative viscosity, *i.e.* $(\eta/\eta_0)^{1/3}$, *vs.* [complex]/[DNA]. η_0 and η are the viscosity of the free DNA solution and the DNA-complex solution, respectively.

2.3.3. Circular dichroism (CD) spectroscopy. Solutions of CT-DNA (200 μM) with [complex]/[DNA] ratios of 0.0, 0.5 and 1.0 were incubated at 37 °C for 24 h. The CD spectra of these solutions were recorded from 200 to 400 nm using a quartz cuvette with an optical path length of 10 mm and a scanning rate of 100 nm min^{-1}. The data were collected in triplicate with a time constant of 1 s and a spectral bandwidth of 1.0 nm. The background signal due to the buffer was subtracted.

2.3.4. DNA-melting analysis. The DNA denaturation experiments in the presence of the copper(II) complexes with [complex]/[DNA] ratios of 0.5, 1.0, 1.5 and 2.0 were performed by monitoring the variation of the absorption intensity of DNA (200 μM) at 259 nm when the temperature of the DNA solution was increased from 25.0 to 100.0 °C. All data were collected at each 5 °C increase and are presented as the normalized absorbance, $(A - A_0)/(A_f - A_0)$, *versus* temperature, where A_f, A_0, and A are the final, the initial, and the observed absorbance at 259 nm, respectively. The melting temperature (T_m) was determined from the maximum of the first derivative curve or tangentially from the graph at the midpoint of the transition curve. ΔT_m was defined as the difference between T_m of the free DNA and T_m of the bound DNA.

2.3.5. Fluorescence spectroscopy. Emission intensity measurements of ethidium bromide (EB) with free CT-DNA in the absence and presence of complexes **1–4** were performed in 3% MeOH/Tris-buffer, pH = 7.2. The CT-DNA solution (50 μM) was pretreated with EB (25 μM) for 30 min at room temperature and stored in the dark. The complex solutions were then prepared (from the previous stock solution of EB–DNA) with [complex]/[DNA] ratios of 0.0 to 1.0 with 0.1 intervals. These solutions were kept in the dark for 30 min before measurement. The emission intensities (between 550 and 700 nm) were obtained through excitation at 500 nm.

To examine the fluorescence quenching mechanism, the Stern–Volmer quenching constant (K_{SV}) was determined by eqn (2).[21]

$$F_0/F = 1 + K_{SV}[Q] \quad (2)$$

where F_0 and F are the fluorescence intensities of the DNA–EB complex in the absence and presence of the copper(II) complexes, respectively. [Q] is the concentration of the complexes.

2.3.6. Determination of stoichiometry of complex–DNA interactions. The copper(II)/DNA complex stoichiometry was determined by a similar procedure to one described in the literature.[22] The complex solution (3 mM, 1 mL) was added to the CT-DNA solution (*ca.* 3 mM, 1 mL), and the resulting mixture was incubated at 37 °C for 24 h. Precipitation of the DNA–copper(II) complex was achieved by adding absolute ethanol (4 mL) and NaCl (2 mM, 0.2 mL) and maintaining the mixture at −70 °C for 1 h. The precipitate was subsequently isolated by centrifugation at 4 °C (10 000 rpm, 30 min). The supernatant was separated by pouring it out slowly. Next, deionized water (25 mL) was added to dissolve the copper(II)/DNA precipitate. The DNA concentration in the obtained DNA–copper(II) complex solution was calculated (from triplicate experiments) by the absorption intensity at 259 nm using ε = 6600 M^{-1} cm^{-1}.[18] The amount of copper(II) was determined by atomic absorption spectroscopy, hence providing the Cu (mmol)/DNA (mol base) ratio.

2.4. DNA cleavage studies

2.4.1. Gel electrophoresis. Electrophoresis experiments were performed using supercoiled plasmid pBR322 DNA. The cleavage reactions of the plasmid DNA (0.2 μg, ~30 μM) were undertaken in two conditions: (i) the addition of **1–4** alone (200, 400, 600 and 800 μM) and (ii) the addition of **1–4** (10 to 400 μM for **1** and **3**; 0.1 to 4.0 μM for **2** and **4**) in the presence of ascorbic acid, H_2ASC (100 μM). The total volume of all samples was adjusted to 10 μL by adding HEPES-buffer (40 mM HEPES and 10 mM $MgCl_2$, pH = 7.2). The samples were incubated at 37 °C for 1 h. Subsequently, loading buffer (2 μL) containing 0.25% bromophenol blue, 0.25% xylene cyanol and 30% glycerol was added to the samples. The resulting mixtures were loaded into 0.8% agarose gel and the fragments of each DNA form were separated by electrophoresis (50 V for 1.5 h in 1× TAE buffer containing 40 mM Tris-acetate and 1 mM EDTA). The gel was stained with ethidium bromide for 5 min and photographed under UV light. The proportion of the DNA forms was estimated by the volume of the visualized DNA bands (volume = intensity × area) and used to determine the extent of DNA cleavage. The intensities of the supercoiled DNA (Form I) were corrected by multiplying by the factor value of 1.22 (for pBR322 DNA) because the intercalation between EB and Form I is relatively weak when compared to that of nicked (Form II) and linear (Form III) DNA.[23] The extent of DNA cleavage activity was calculated by eqn (3).[24]

$$\%\text{DNA cleavage activity} = \{[(\text{volume of DNA-Form I})_{\text{control}} - (\text{volume of DNA-Form I})_{\text{sample}}]/(\text{volume of DNA-Form I})_{\text{control}}\} \times 100 \quad (3)$$

2.4.2. Atomic-force microscopy (AFM). Plasmid pBR322 DNA (0.2 μg), heated at 60 °C for 15 min to open the supercoiled DNA, was incubated with the copper(II) complexes (400 μM for **1** and **3**; 4.0 μM for **2** and **4**) in the presence of H_2ASC (100 μM) in 20 μL HEPES-buffer at 37 °C for 1 h. Milli-Q water and all solutions for the AFM studies were filtered through 0.2 μm FP030/3 filters (Scheicher and Schuell GmbH, Germany) to obtain clear AFM images. After incubation, a drop (8 μL) of each sample was placed onto peeled mica disks (PELCO Mica Discs, 9.9 mm diameter; Ted Pella, Inc. California, USA) and allowed to adsorb for 2 min at room temperature. The samples were rinsed for 5 s with a stream of Milli-Q water directly onto the surface, which was subsequently blown dry with compressed argon before imaging.

2.5. Cytotoxicity assay

Cancer-cell growth inhibition of the copper(II) complexes against three human cancer cell lines, namely KB (epidermoid carcinoma of oral cavity, ATCC CCL-17), MCF-7 (breast adenocarcinoma, ATCC HTB-22) and NCI-H187 (small cell lung carcinoma, ATCC CRL-5804), was determined using the Resazurin Microplate assay (REMA) as previously described.[25] Ellipticine, doxorubicin and tamoxifen were used as positive controls, and 0.5% DMSO was used as a negative control. To investigate the potential cytotoxic behaviors of the copper(II) complexes, cells at a logarithmic growth phase were harvested and diluted in fresh medium to 7×10^4 cells mL^{-1} for KB and 9×10^4 cells mL^{-1} for MCF-7 and NCI-H187. Successively, 5 μL of the test sample diluted in 5% DMSO and 45 μL of cell suspension were added to 384-well plates and then incubated at 37 °C in a 5% CO_2 incubator. After the incubation period (3 days for KB and MCF-7, and 5 days for NCI-H187), 12.5 μL of 62.5 μg mL^{-1} resazurin solution was added to each well, and the plates were then incubated at 37 °C for 4 h. The fluorescence signal was measured using a SpectraMax M5 multi-detection microplate reader (Molecular Devices, USA) at excitation and emission wavelengths of 530 nm and 590 nm, respectively. Percentage inhibition of the cell growth was calculated by eqn (4).

$$\%\text{Inhibition} = [1 \times (FU_T/FU_C)] \times 100 \quad (4)$$

where FU_T and FU_C are the mean fluorescence units under the treated and untreated conditions from the copper(II) complexes, respectively. The anticancer activity of the complexes was expressed as 50% of the inhibitory concentration (IC_{50}) determined from the dose–response curves using SOFTMax Pro software (Molecular Devices, USA). The plotted data were obtained from 6 concentrations of 2 fold serially diluted test samples. The complexes with IC_{50} > 50 μg mL^{-1} were considered to be inactive.[26]

2.6. Antibacterial activity studies

The screening of the *in vitro* antibacterial activity of the copper(II) complexes (50 mg mL^{-1}) against three Gram-negative bacteria (*Salmonella*, *E. coli* and *Campylobacter*) was performed using the agar-well diffusion method.[27] Active culture of the bacteria was transferred into 0.75% (w/w) semisolid brucella agar (10 mL) at 50 °C. Subsequently, the incubated medium was swirled to distribute the cell culture of bacteria and was maintained at room temperature for 30 min. A well 6 mm in diameter was made aseptically. The plates were maintained at 37 °C for 48 h under appropriate conditions to allow cell culture growth. Each complex was dissolved in 3% MeOH/Tris-buffer, pH = 7.2 to a final concentration of 1000 μg mL^{-1} and transferred aseptically

into a well. The inhibitory activity of the complex on bacteria was obtained from the clear zone around the disc. The minimum inhibitory concentration (MIC) values were also determined by two-fold serial dilution in liquid media containing the tested complexes.[28] The experiments were carried out in duplicate.

3. Results and discussion

3.1. Complex preparation

3.1.1. General chemistry. Our previous study reported the interesting biological properties and cytotoxicity of copper(II) chloride complexes containing 1-amidino-*O*-methylurea (L^1) and *N*-(benzyl)-amidino-*O*-methylurea (L^2), $[Cu(L^1)Cl_2]_2$ and $[Cu(L^2)Cl_2]_2$.[16] This behaviour led us to further investigate those two copper(II) compounds with the addition of another ligand to improve their activities. N,N-Heterocyclic ligands, 2,2′-bipyridine (bipy) and 1,10-phenanthroline (phen), were selected due to their planar geometries and various beneficial biological activities (*e.g.* antitumor, antifungal, antiviral and antimycoplasmal activities).[29–32] Herein, four new complexes (**1–4**) were prepared by the reaction of the blue dimeric complexes $[Cu(L^1)Cl_2]_2$ or $[Cu(L^2)Cl_2]_2$ with bipy or phen in a 1 : 2 molar ratio at pH 7 in MeOH.

The colors of all four products changed, from blue to purple for **1**, **2** and **4** and from blue to pink for **3**, indicating that the environments around the copper(II) centers differ from those of the starting compounds. This change was the first evidence indicating that the reactions took place. To gain more information to confirm the formation of **1**, **2**, **3** and **4**, various techniques were utilized, including infrared spectroscopy, elemental analysis, mass spectrometry, diffuse reflectance, UV-Vis and electron paramagnetic resonance (EPR) spectroscopies.

The infrared spectra of complexes **1–4** (Fig. 1) exhibit the characteristic bands of both chelating N,N-heterocyclic ligands and the corresponding starting complexes. Strong, broad splitting bands at 3486 to 3208 cm^{-1} are assigned to the N–H stretching vibrations of the ligands L^1 and L^2.[16] The N–H bending vibrations shifted from 1692 to 1656 cm^{-1} to lower frequencies at 1643 to 1589 cm^{-1} upon the coordination of the heterocyclic ligands. This situation was also found in our previous report.[16] This behavior indicates the existence of the ligands L^1 and L^2 in the products. Upon chelation of bipy and phen, the ring stretching vibrations of the C=C and C=N functional groups of free bipy (1578 to 1415 cm^{-1}) and phen (1503 to 1421 cm^{-1}) were found to be shifted to higher frequencies at 1583 to 1448 cm^{-1} for **1** and 1589 to 1451 cm^{-1} for **3** (Fig. 1a), as well as 1523 to 1428 cm^{-1} for **2** and 1524 to 1427 cm^{-1} for **4** (Fig. 1b). Additionally, the characteristic out-of-plane bending modes of free bipy (755 to 740 cm^{-1}) shifted to 771 cm^{-1} for **1** and 756 to 708 cm^{-1} for **3**, while those of free phen (853 to 738 cm^{-1}) shifted to 851 to 722 cm^{-1} for **2** and 843 to 719 cm^{-1} for **4**. Moreover, peaks assigned to the C–H bending vibration of the phenyl ring on the sidearm of the L^2 ligand at 1385 to 1226 cm^{-1} were also presented at 1394 to 1250 cm^{-1}. The changes in the vibrational energies of the functional groups upon complexation indicate the coordination of the two heterocyclic nitrogen donor atoms of bipy and phen[33] with the copper center of the starting complex.

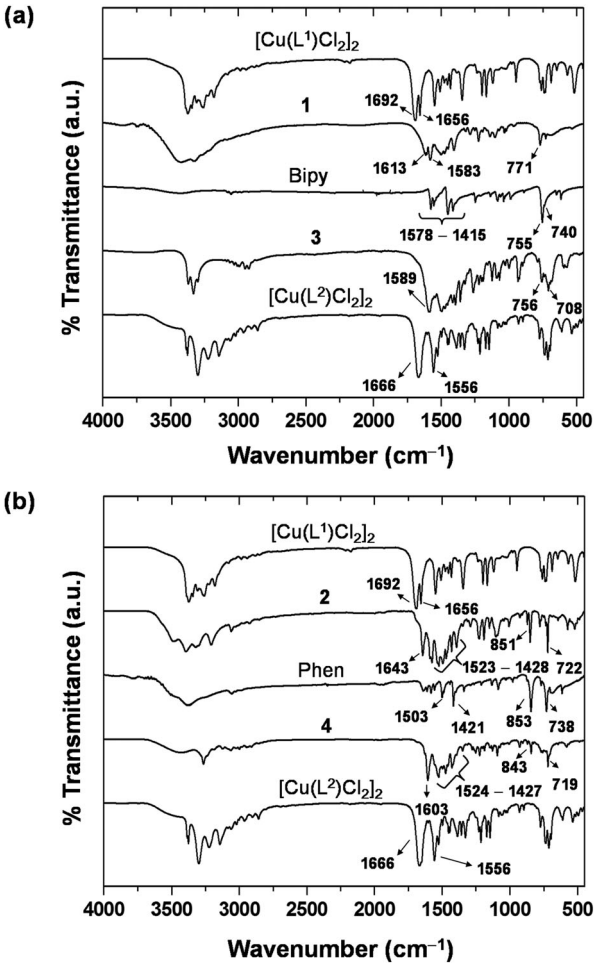

Fig. 1 Overlayered FT-IR spectra of (a) **1** and **3**, and (b) **2** and **4** compared with the starting complexes and the secondary chelating N,N-heterocyclic ligands (bipy and phen).

3.1.2. Prediction of the chemical formulas of the copper(II) complexes. Data from elemental analysis shows that the percentages of carbon, hydrogen and nitrogen of all four products are in good agreement with the chemical formulae of the desired copper(II) complexes, $[Cu(L^1)(bipy)]Cl_2$ (**1**), $[Cu(L^1)(phen)]Cl_2$ (**2**), $[Cu(L^2)(bipy)Cl_2]$ (**3**) and $[Cu(L^2)(phen)]Cl_2$ (**4**).

Additionally, the compositions of the products were interpreted from ESI+ mass spectra (Fig. S1–S4, ESI†). The ion peaks are listed in Table 1. The relative molecular ion peaks, *i.e.* $[Cu(L^1)(bipy)]^{2+}$ (m/z = 335) for **1**; $[Cu(L^1)(phen)]^{2+}$ (m/z = 359) for **2**; $[Cu(L^2)(bipy)Cl_2 + 2H]^{2+}$ (m/z = 497) for **3**; and $[Cu(L^2)(phen)]^{2+}$ (m/z = 449) for **4** were observed. Additionally, the molecular fragment ions related to the ligands and the relative abundance of the isotopes of ^{63}Cu and ^{65}Cu were also found in the spectra. Hence, the obtained evidence leads us to conclude that four new copper(II) compounds have been achieved. Furthermore, the ion species of copper-bipy or copper-phen complexes which

Table 1 ESI+ mass spectral data for **1–4**

Complex	*m*/*z*	Interpretation
$[Cu(L^1)(bipy)]Cl_2$ (**1**)	411	$[Cu(bipy)_2Cl + H]^{2+}$
	376	$[Cu(bipy)_2 + H]^{2+}$
	335	$[Cu(L^1)(bipy)]^{2+}$
	322	$[Cu(bipy)Cl_2 + H + CH_3OH]^{+}$
	173	$[L^1 + Na + 2H + CH_3OH]^{3+}$
	158	$[bipy + 2H]^{2+}$
	151	$[L^1 + 3H + CH_3OH]^{3+}$
	119	$[L^1 + 3H]^{3+}$
$[Cu(L^1)(phen)]Cl_2$ (**2**)	458	$[Cu(phen)_2Cl]^{+}$
	424	$[Cu(phen)_2 + H]^{2+}$
	403	$[Cu(L^1)(phen) + CO_2]^{2+}$
	359	$[Cu(L^1)(phen)]^{2+}$
	322	$[Cu(phen)Cl + CO_2]^{+}$
	182	$[phen + 2H]^{2+}$
	173	$[L^1 + Na + 2H + CH_3OH]^{3+}$
$[Cu(L^2)(bipy)Cl_2]$ (**3**)	497	$[Cu(L^2)(bipy)Cl_2 + 2H]^{2+}$
	475	$[Cu(L^2)_2]^{2+}$
	449	$[Cu(bipy)_2Cl_2 + 4H]^{4+}$
	424	$[Cu(L^2)(bipy)–H]^{+}$
	400	$[Cu(bipy)_2 + 2H + Na]^{4+}$
	376	$[Cu(bipy)_2 + H]^{2+}$
	208	$[L^2 + 2H]^{2+}$
	158	$[bipy + 2H]^{2+}$
$[Cu(L^2)(phen)]Cl_2$ (**4**)	458	$[Cu(phen)_2Cl]^{+}$
	449	$[Cu(L^2)(phen)]^{2+}$
	424	$[Cu(phen)_2 + H]^{2+}$
	337	$[Cu(phen)Cl_2 + Na + H]^{2+}$
	314	$[Cu(phen)Cl_2 + H]^{+}$
	206	$[L^{2\bullet}]^{+}$
	182	$[phen + 2H]^{2+}$

appeared in the spectra were probably formed in the ionization process during analysis.[34–37]

3.1.3. Prediction of the possible geometry of the copper(II) complexes. After several attempts, suitable single crystals of the complexes in this system were not achieved. Hence, electronic absorption and X-band EPR spectroscopic methods were utilized to predict their coordination geometries.

3.1.3.1. Electronic absorption spectra. Absorption spectra of **1–4** in the solid and solution phases were recorded (Fig. S5, ESI† and Table 2). In the solid state, the spectra of the purple complexes (**1**, **2** and **4**) are similar and exhibit a strong band in the visible region at 526 to 567 nm (19 029 to 17 643 cm^{-1}) (Fig. S5a, b and d, ESI†). Meanwhile, the spectrum of the pink complex **3** is different; it shows two overlapping absorption bands at 492 nm (20 300 cm^{-1}) and 560 nm (17 643 cm^{-1}) (Fig. S5c, ESI†). In addition, the spectra of **1–4** were compared with those of the square pyramidal starting compounds ($[Cu(L^1)Cl_2]_2$ and $[Cu(L^2)Cl_2]_2$), which are blue in color and have d–d transition bands at 618 to 665 nm (16 175 to 15 049 cm^{-1}).[11,16] The changes in color from blue for the starting compounds to purple or pink for **1–4**, together with a considerable blue shift, preliminarily suggest that the four complexes have different coordination geometries and environments surrounding their copper(II) centers than the initial compounds. According to these results, the electronic absorption of **1**, **2** and **4** may be attributed to a square planar geometry with the CuN_4 chromophore,[38–40] which may arise from the replacement of chloride in $[Cu(L^1)Cl_2]_2$ and $[Cu(L^2)Cl_2]_2$ by two nitrogen donor atoms of the heterocyclic molecule, resulting in the shift to shorter wavelength of the d–d absorption bands of 139 nm (for **1**), 132 nm (for **2**) and 51 nm (for **4**). Meanwhile, the electronic spectrum of complex **3** indicates that its molecular geometry may adopt a distorted octahedron.[39,41] Further evidence to support the proposed geometry of **3** is the electronic spectra of the distorted octahedral copper(II) complexes of ethylenediamine and derivatives with the same CuN_4Cl_2 chromophore, which exhibit a broad band at 520 to 532 nm (19 200 to 18 800 cm^{-1}) with a shoulder at 581 to 585 nm (17 200 to 17 100 cm^{-1}),[41,42] similar to the absorption of **3**.

Moreover, it is essential to investigate the effect of solvents on the structures of the complexes **1–4** to further confirm their possible geometries. Due to the poor water solubility of **3** and **4**, the electronic absorption spectra of all complexes were recorded in MeOH and DMSO. The color changes of **1**, **2** and **4** from purple in the solid state to purplish blue in MeOH and green in DMSO are caused by the shift of the absorption bands (Table 2). This result suggests that their coordination geometries in the solid state differ from those in solution phase due to solvation effects. This leads us to conclude that **1**, **2** and **4** in the solid state are highly capable of adopting a square planar geometry containing vacant sites at the axial positions that are available for solvents. In the case of **3**, its spectra in the solid state and in both organic solvents are somewhat altered. However, the pink color of both phases apparently remains unchanged, suggesting that the solvent molecules do not interact with the copper(II) center. This behavior strengthens the conclusion that the coordination geometry of **3** is a distorted octahedron.

3.1.3.2. EPR spectra. X-band EPR spectra provide alternative information to further confirm the stereochemistry of the copper(II) complexes. All the complexes exhibit anisotropic spectra with hyperfine splitting lines around the $g_{\parallel}$ region due to the interaction of the $S = 1/2$ electron spin with the $I = 3/2$ copper nucleus (Fig. 2). The spin Hamiltonian parameters, g tensor values, describing the electronic ground state of the copper center, show $g_{\parallel} > g_{\perp} > 2.0$, which is indicative of a $d_{x^2-y^2}$ ground state corresponding to elongated tetragonal octahedral or square planar geometries (Table 2).[43] Obviously, it is difficult to distinguish between the components of the $g_{\parallel}$ peak because of the overlap with the $g_{\perp}$ peaks. Moreover, minor signals between the $g_{\parallel}$ components are found in the spectra of **1**, **2** and **4**. This may be due to the interactions between the complexes and the solvent molecules, as was likely observed in our previous report.[16] The parallel hyperfine coupling constant ($A_{\parallel}$) in the range of 201 to 207 G supports a square-planar CuN_4 geometry in complexes **1**, **2** and **4**,[40] while that of **3** ($A_{\parallel}$ = 216 G), showing a larger value together with a lower $g_{\parallel}$ value, is characteristic of tetragonally elongated pseudooctahedral copper(II) complexes.[44,45] In comparison with the starting compounds, changes in the spin Hamiltonian parameters (a decrease in $g_{\parallel}$ and an increase in $A_{\parallel}$) are observed because the two chloride ligands in $[Cu(L^1)Cl_2]_2$ or

Table 2 Electronic absorption and EPR spectral data of **1–4**

	Electronic spectra, λ_{max}, $1/\lambda_{max}$ (nm, cm^{-1})					Spin Hamiltonian parameters				
Complex	Solid	Appearance	MeOH	Appearance	DMSO	Appearance	$g_{\parallel}$	$g_{\perp}$	$A_{\parallel}$ (G)	A_N (G)
$[Cu(L^1)Cl_2]_2$[a]	665, 15 049[b]	Light blue	680, 14 710	Blue	674, 15 528	Green	2.28	2.06	168	—
1	526, 19 029	Purple	588, 17 123	Purplish blue	572, 17 123 694, 14 409	Green	2.18	2.04	203	14.8
2	533, 18 754	Purple	585, 17 094	Purplish blue	581, 17 212 704, 14 205	Green	2.17	2.05	207	15.3
$[Cu(L^2)Cl_2]_2$[a]	618, 16 175[b]	Deep blue	705, 14 180	Blue	624, 16 025 936, 10 684	Green	2.27	2.06	158	—
3	492, 20 300 560, 17 857	Pink	525, 19 048	Pink	489, 20 471	Pink	2.15	2.05	216	17.6
4	567, 17 643	Purple	587, 17 036	Purplish blue	585, 17 094 697, 14 347	Green	2.17	2.05	201	15.1

[a] The starting complexes. [b] Data from ref. 16.

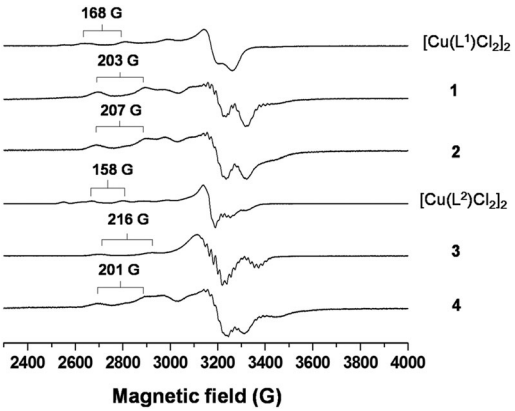

Fig. 2 X-band EPR spectra in frozen DMSO solution of complexes **1–4** compared with the starting complexes $[Cu(L^1)Cl_2]_2$ and $[Cu(L^2)Cl_2]_2$ at 77 K.

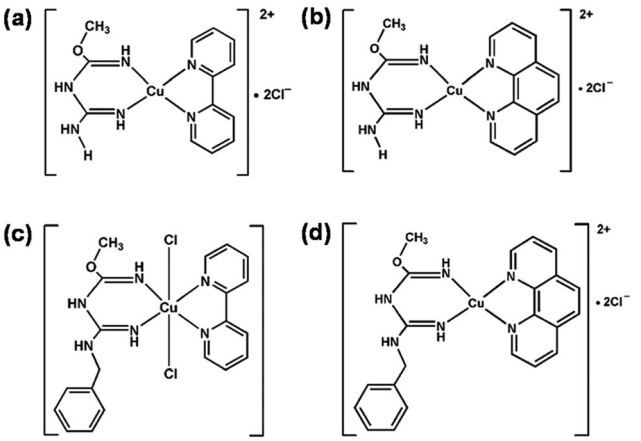

Fig. 3 Possible geometries of (a) **1**, (b) **2**, (c) **3** and (d) **4**.

$[Cu(L^2)Cl_2]_2$ are replaced by two nitrogen donors of the N,N-heterocyclic ligands, yielding CuN_4 based complexes. A similar behavior was found in our previous studies.[16] Moreover, a typical superhyperfine interaction of the unpaired electron of the copper ion with four magnetically ^{14}N nucleases (I = 1) is found in their spectra at the $g_{\perp}$ region, with superhyperfine coupling values (A_N) of 15 to 18 G (Table 2). These parameters are close to those observed for the copper(II) ion coordinated in the equatorial plane by four strong nitrogen donors provided by chelating ligands.[16,46,47] On the other hand, this coupling is unobservable in the starting complexes $[Cu(L^1)Cl_2]_2$ and $[Cu(L^2)Cl_2]_2$ (Fig. 2).

The electronic absorption spectra and the spin Hamiltonian parameters derived from the experimental EPR spectra allow us to identify the possible geometries of the copper(II) complexes (Fig. 3). The proposed structures of **1**, **2** and **4** may adopt similar square planar geometries, with four nitrogen donor atoms from the ligand L^1 or L^2 and the heterocycles (bipy or phen), yielding a CuN_4 coordination sphere. In contrast, a different coordination structural arrangement is found for **3**, which possibly adopts a CuN_4Cl_2 octahedral geometry. The predicted coordination geometries of all the complexes may provide a better understanding of the properties related to their biological activities.

3.2. DNA-binding studies of complexes 1–4

An essential property leading to the biological applications of complexes is their DNA-binding behaviors. In principle, these binding interactions are classified into two modes, covalent and non-covalent. The former mode is found in cisplatin, a well-known covalent DNA-binder which interacts with DNA through coordinate covalent bonds at N7 of guanine on the DNA strand.[3] There are three major pathways for the later mode; (i) intercalative binding between two adjacent base pairs perpendicular to the helical axis, (ii) outside-edge binding to the sugar–phosphate backbone of the helix through electrostatic interactions and (iii) groove binding at either the major or minor groove *via* hydrophobic interactions and hydrogen bonding.[48] Sufficient evidence is necessary to predict the main DNA-binding modes. Thus, the DNA-binding behavior and the possible DNA-binding modes of **1–4** toward CT-DNA were intensively investigated by many methods.

3.2.1. Electronic absorption titration. The changes observed in the electronic absorption spectra of the complexes upon addition of different concentrations of DNA can be used to predict their possible DNA-binding modes. Ethidium bromide (EB), which is known as a DNA intercalating agent, is used as a reference. The hypochromic effect associated with redshift arises

from an intercalative mode involving the strong π → π* stacking interaction between the planar aromatic ligands of the complexes and DNA base pairs.[49,50] Conversely, the hyperchromic effect may be attributed to two possible causes: (i) the complexes can bind with DNA *via* external contact (electrostatic binding),[51] or (ii) they partially uncoil the DNA helical structure and expose more bases embedded in the DNA.[52] These interactions involve non-intercalative modes which cause alterations of the DNA duplex structure.[53] The absorption spectra of **1–4** exhibit absorption bands in the range of 200 to 350 nm which are assigned to π → π* intraligand transitions (Fig. 4).[54] Upon titration with CT-DNA at [complex]/[DNA] ratios of 0.67 to 5.00, a decrease in absorbance (hypochromism) with redshift is observed in the spectra of all the complexes. This behavior is most likely similar to that observed for a classical intercalator, EB (Fig. 4a), but is in contrast to the starting compounds[12] and other related complexes of amidino-*O*-alkylurea derivatives, which have been reported as non-intercalating agents (Table 3).[10,55–57]

The binding strength of the complexes with CT-DNA can be evaluated by the values of the intrinsic binding constant (K_b), which are obtained by monitoring the change in absorbance at 302 nm for **1**, 204 nm for **2**, 300 nm for **3** and 203 nm for **4**. The calculated K_b values are found to be in the order of EB > **2** > **4** > **1** > **3**. In comparison with their starting compounds,

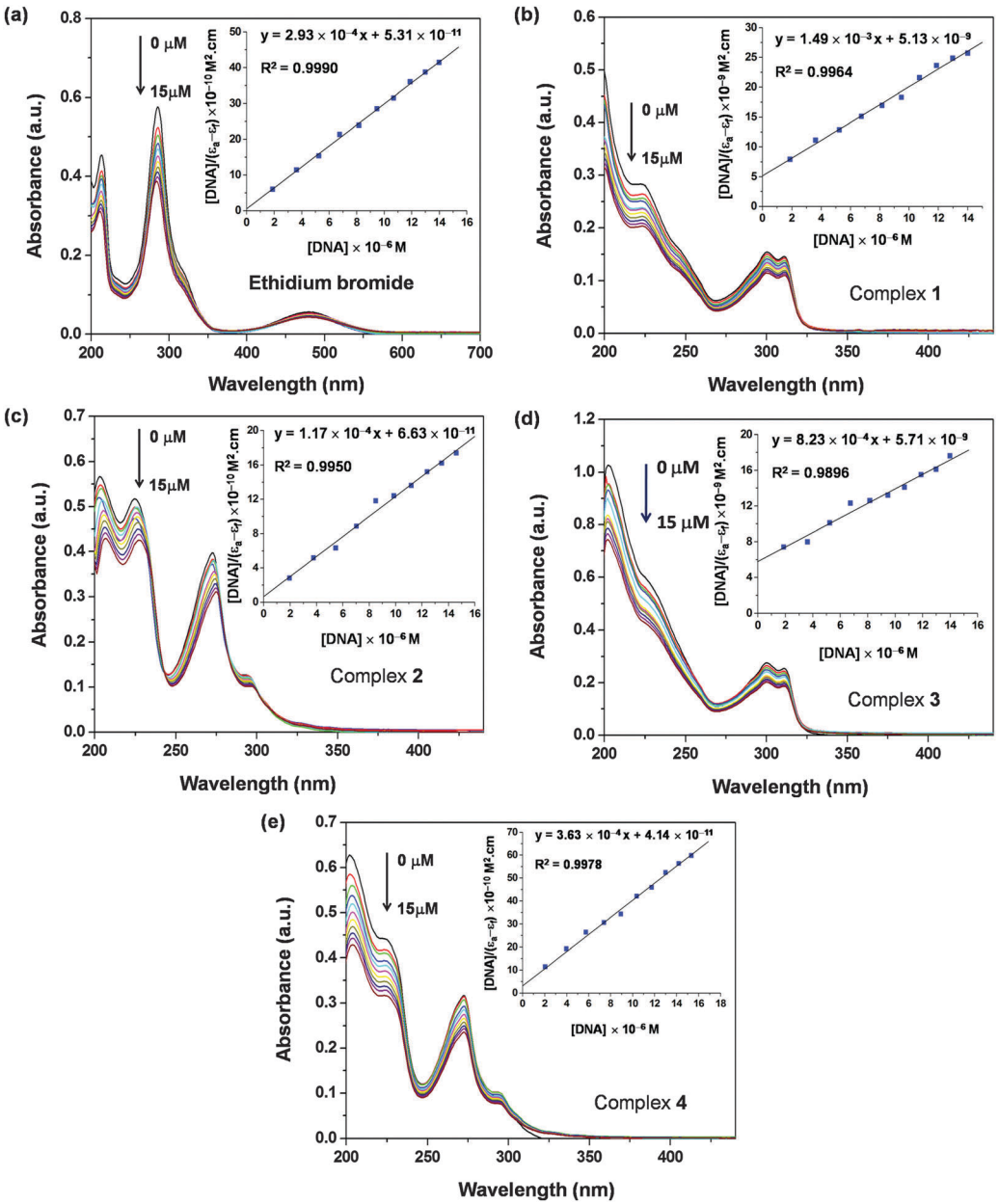

Fig. 4 Absorption spectra of ethidium bromide (a) and complexes **1–4** (10 μM) (b–e) in the absence (—) and presence of increasing amounts of DNA (2 to 15 μM) after incubation at 37 °C for 24 h. The arrows show the absorbance changes upon the addition of the DNA concentrations. Insets: Linear plot of [DNA]/($\varepsilon_a - \varepsilon_f$) *vs.* [DNA] for the titration of the copper(II) complexes with DNA.

Table 3 Electronic absorption data of **1–4**, the starting compounds ($[Cu(L^1)Cl_2]_2$ and $[Cu(L^2)Cl_2]_2$) and other related copper(II) compounds with increasing amount of CT-DNA

Complex	Absorption, λ (nm)	Change in absorptivity[a]	Shift (nm)	K_b (M^{-1})	Ref.
Ethidium bromide (EB)	285	—	+1	5.52×10^6	This work
$[Cu(L^1)Cl_2]_2$	226	+	−2	5.63×10^4	12
$[Cu(L^2)Cl_2]_2$	209	+	−5	1.07×10^5	12
$[Cu(L^1)(bipy)]Cl_2$ (**1**)	302	—	+2	2.90×10^5	This work
$[Cu(L^1)(phen)]Cl_2$ (**2**)	204	—	+4	1.76×10^6	This work
$[Cu(L^2)(bipy)Cl_2]$ (**3**)	300	—	+1	1.44×10^5	This work
$[Cu(L^2)(phen)]Cl_2$ (**4**)	203	—	+1	8.77×10^5	This work
$[Cu(L^1)_2]Cl_2$	228	+	0	5.67×10^4	10
$[Cu(L^2)_2]Cl_2$	229	+	−1	1.16×10^5	10
$[Cu(L^3)_2](ClO_4)_2 \cdot H_2O$[b]	224	+	−2	4.08×10^4	55
$[Cu(L^4)_2](ClO_4)_2 \cdot 2/3H_2O$[c]	224	+	−2	1.39×10^4	55
$[Cu(L^5)_2](ClO_4)_2 \cdot H_2O$[d]	225	+	−3	3.06×10^4	55
$[Cu(bipy)_2]^{2+}$	NR[e]	NR[e]	NR[e]	3.24×10^4	56
$[Cu(phen)_2]^{2+}$	NR[e]	NR[e]	NR[e]	2.75×10^3	57

[a] + = hyperchromism; − = hypochromism. [b] L^3 = 1-amidino-*O*-2-methoxyethylurea. [c] L^4 = 1-amidino-*O*-2-ethoxyethylurea. [d] L^5 = 1-amidino-*O*-2-buthoxyethylurea. [e] NR = not reported.

which bind to DNA through non-intercalative interactions, all four complexes have higher binding potentials. Moreover, they show greater binding strength than other related compounds (Table 3). This result indicates that the incorporation of the L^1 or L^2 ligands with N,N-heterocyclic ligands enhances the efficiency of their interaction with DNA.

To compare the DNA-binding strength of all four complexes in the present work, their K_b values are considered. In general, the degree of the intercalative property of a complex depends on the existing aromatic heterocyclic ring, which can insert and stack between the base pairs of DNA. The extension of planarity in the intercalating ligand may strengthen the interaction of the complex with DNA.[58] The obtained results suggest that the complexes in our system can bind to DNA through an intercalative mode with different binding potentials. The higher K_b values of the complexes containing phen (**2** and **4**) compared to the complexes containing bipy (**1** and **3**) may be due to the greater planar area and extended π system of phen compared to bipy. Hence, phen provides more planarity for **2** and **4** and enables their stronger intercalative interactions with DNA compared to **1** and **3**.

Complex **3** gives the lowest K_b value, meaning it has the weakest DNA-binding strength. This may be caused by its structure, which is proposed as an octahedron according to the spectroscopic results (electronic absorption and EPR). This geometry causes the molecule of **3** to have less planarity, thus resulting in weaker interactions with DNA than the remaining three compounds (**1**, **2** and **4**), which are proposed to be square planar. To confirm their DNA-binding behaviors, it was necessary to carry out further experiments.

3.2.2. Viscometric measurements. To further investigate the DNA-binding modes of the complexes, viscometric assays, which measure the flow time of CT-DNA solutions with increasing amounts of the complexes, were carried out. Basically, partial and/or non-classical intercalation of the complexes may bend (or kink) the DNA helix, resulting in the reduction of its effective length and, concomitantly, its viscosity.[59] Fig. 5 illustrates the plot of the relative viscosity of DNA in the presence and absence

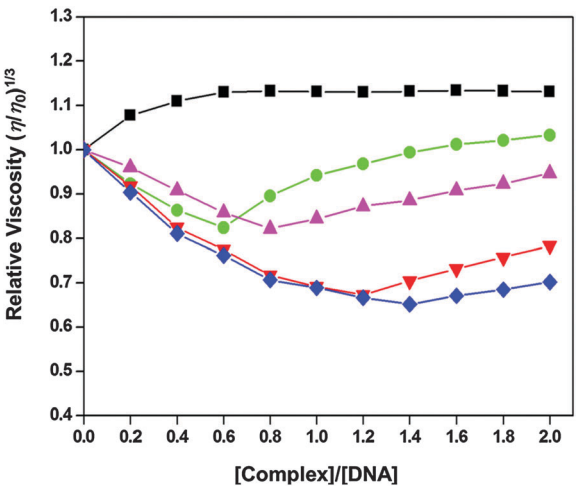

Fig. 5 Influence of increasing amounts of ethidium bromide (–■–), complexes **1** (–▼–), **2** (—●—), **3** (–◆–) and **4** (–▲–) on the relative viscosity of CT-DNA (200 μM) at 37 °C.

of the complexes. Ethidium bromide (EB), an intercalator used as a reference, can enhance the relative viscosity of DNA in [EB]/[DNA] ratios of 0.0 to 0.6, due to increasing separation of the DNA base pairs and lengthening of the DNA helix upon intercalation. When [EB]/[DNA] ≥ 0.8, the relative viscosity is nearly constant because the binding sites on DNA may reach saturation. In the presence of complexes **1–4**, two different behaviors depending on the [complex]/[DNA] ratios are observed. Firstly, the reduction in the relative viscosity of DNA, which shows the opposite trend to EB, is observed in the range of [complex]/[DNA] = 0.0 to 1.2 for **1**; 0.0 to 0.6 for **2**; 0.0 to 1.4 for **3**; and 0.0 to 0.8 for **4** (Fig. 5). This behavior points to a non-intercalative binding mode. Lastly, an enhancement of the relative viscosity of DNA is observed when the [complex]/[DNA] ratio increases from 1.2 to 2.0 for **1**; 0.6 to 2.0 for **2**; 1.4 to 2.0 for **3**; and 0.8 to 2.0 for **4**. The higher [complex]/[DNA] ratios give similar results to EB at low concentration, suggesting that the complexes have changed their DNA-interacting behavior to an intercalative binding mode.

It is noted that the effects of **1–4** on the DNA viscosity are different for both the decreasing and increasing ranges. In the decreasing range, complexes **1** and **3** predominantly show the broader range of the [complex]/[DNA] ratios; they reduce the degree of DNA viscosity more than **2** and **4**. In the increasing range, complexes **2** and **4** clearly exhibit increasing enhancement of the viscosity, close to that of EB, in a wider range of [complex]/[DNA] ratios than **1** and **3**. Under these experimental conditions, the results demonstrate that intercalative interaction maybe a major DNA-binding mode for the complexes containing phen (**2** and **4**). In contrast, non-intercalative interactions, *i.e.* electrostatic interactions, partial intercalation and/or groove binding, may be a main binding mode for the complexes containing bipy (**1** and **3**). These behaviors denote that the DNA-binding interactions of the complexes depend on the [complex]/[DNA] ratio.

3.2.3. Circular dichroism spectra. The effect of metal complexes on the secondary structure of DNA can provide good evidence about their potential interactions with these biomolecules. To observe these changes, circular dichroism (CD) signals, which are quite sensitive to DNA-binding modes,[60] were determined at [complex]/[DNA] ratios of 0.5 and 1.0. Generally, the CT-DNA typed B-form shows a CD signal with two characteristic bands, including a positive band at 275 nm that is attributable to base stacking and a negative band at 245 nm arising from the right-handed helicity of the DNA.[61] Observed modifications of either a change in the band position or intensity, or even both, in the CD spectra of DNA in the presence of the complexes can be correlated to their interactions. Simple electrostatic interactions or groove binding between the complexes and DNA cause little or no perturbation of the base stacking and helicity bands, whereas classical intercalation can stabilize the double helical conformation of B-DNA and enhance the intensities of both CD bands, as observed for the classical intercalator ethidium bromide (EB) (Fig. S6a, ESI†).

In this study, the characteristic CD bands of all the complexes alone are almost unobservable. After incubation of the complexes in the presence of DNA, changes in the CD spectra of the DNA are observed. These changes indicate some modifications in the secondary structure of DNA by **1–4** (Fig. S6b–e, ESI†). The variations of wavelength ($\Delta\lambda_{max/min}$) and ellipticity ($\Delta\theta_{max/min}$) for both the positive and negative bands are listed in Table 4. Addition of **1** gradually decreases the ellipticity signals of both CD bands, along with a redshift (Fig. S6b, ESI†). Similar modifications can also be found for complex **3** (Fig. S6d, ESI†). On the other hand, complexes **2** and **4** produce a significant increase in the intensity of the positive band, with a small redshift, and a slight decrease in the intensity of the negative band (Fig. S6c and e, ESI†).

These observable effects of **1–4** on the DNA structure suggest that their interactions with DNA may be different. Under the conditions in this study, the slight perturbations caused by **1** and **3** are clearly opposite to the effect of EB (Fig. S6a, ESI†); therefore, their interactions with DNA are proposed to be non-intercalative. The effects of **1** and **3** on DNA are also analogous to those of the starting complexes $[Cu(L^1)Cl_2]_2$ and $[Cu(L^2)Cl_2]_2$.[12] Meanwhile, the effects of **2** and **4** are dissimilar to **1** and **3** but are similar to some metal complexes containing 1,10-phenanthroline.[57,58] A large increase in the intensity of the positive band possibly involves intercalative interactions stabilized by π–π stacking interactions of the complexes with the base pairs of the double helix.[58] However, a moderate decrease in the intensity of the negative band is indicative of unwinding of the helical DNA structure by the complexes, leading to the loss of some helicity and encouraging a transformation to a more A-like DNA conformation.[57]

3.2.4. DNA-melting study. Additional evidence for the possible DNA-binding behavior of **1–4** can be obtained from thermal denaturation studies. When the temperature of the DNA solution increases, the double-stranded DNA slowly dissociates to single strands, mirrored by a hyperchromic effect at 259 nm. The interaction of a small molecule with DNA can be observed from the alteration of the melting temperature (T_m), depending on its binding affinity. It is known that an intercalating molecule gives rise to stabilization of the DNA helix, indicated by a large increase in the T_m value, while a non-intercalating molecule providing a lower DNA-affinity may produce a small change in the T_m value ($\Delta T_m < 3$ °C).[10,12,62]

All four complexes reveal tendencies to increase the T_m of DNA (81.1 °C) with increasing [complex]/[DNA] ratios (Fig. S7, ESI† and Table 5), indicating interactions between DNA and the complexes. Noticeably, the degree of enhancement of ΔT_m directly depends on the [complex]/[DNA] ratio of each compound. The small change of ΔT_m induced by **1** occurs at [complex]/[DNA]

Table 4 Ellipticity (mdeg) and wavelengths (nm) for the interactions of CT DNA (200 μM) with the copper(II) complexes

		Positive band				Negative band			
Complex	[Complex]/[DNA]	λ_{max}	$\Delta\lambda_{max}$	θ_{max}	$\Delta\theta_{max}$	λ_{min}	$\Delta\lambda_{min}$	θ_{min}	$\Delta\theta_{min}$
DNA		275		15.86		245		−18.82	
Ethidium bromide	0.5	273	−2	24.64	+8.78	247	+2	−35.57	+16.75
	1.0	272	−3	41.94	+26.08	247	+2	−61.51	+42.69
$[Cu(L^1)(bipy)]Cl_2$ (**1**)	0.5	277	+2	14.65	−1.21	246	+1	−17.25	−1.57
	1.0	276	+1	14.88	−0.98	245	0	−12.76	−6.06
$[Cu(L^1)(phen)]Cl_2$ (**2**)	0.5	279	+4	33.77	+17.91	249	+4	−14.84	−3.98
	1.0	281	+6	36.88	+21.02	250	+5	−12.79	−6.03
$[Cu(L^2)(bipy)Cl_2]$ (**3**)	0.5	280	+5	13.54	−2.32	246	+1	−18.20	−0.62
	1.0	279	+4	12.95	−2.91	246	+1	−17.86	−0.96
$[Cu(L^2)(phen)]Cl_2$ (**4**)	0.5	279	+4	30.05	+14.19	248	+3	−16.68	−2.14
	1.0	281	+6	34.58	+18.72	249	+4	−15.81	−3.01

Table 5 Melting temperature of CT DNA in the presence of the complexes at different [complex]/[DNA] ratios

	T_m (°C)				ΔT_m[a] (°C)			
[Complex]/[DNA]	**1**	**2**	**3**	**4**	**1**	**2**	**3**	**4**
0.5	81.9	82.1	81.5	81.7	+0.8	+1.0	+0.4	+0.6
1.0	82.2	84.0	82.1	83.4	+1.1	+2.9	+1.0	+1.3
1.5	82.6	84.6	82.8	84.4	+1.5	+3.5	+1.7	+3.3
2.0	84.3	87.5	83.2	84.7	+3.2	+6.4	+2.1	+3.6

[a] T_m of CT DNA = 81.1 °C.

ratios of 0.5 to 1.5. In addition, similar behavior to the former compound can also be observed at [complex]/[DNA] ratios of 0.5 for **2** and 0.5 to 1.0 for **4**, suggesting that the DNA-binding modes of **1**, **2** and **4** at those [complex]/[DNA] ratios is most likely non-intercalative. When the [complex]/[DNA] ratio of 2.0 is reached, the three compounds again show an enhancement of T_m with $\Delta T_m > 3$ °C, indicating a different DNA-binding behavior, probably intercalation. Differently, the T_m values of DNA solutions in the presence of **3** gradually increase upon increasing [complex]/[DNA] ratio with $\Delta T_m < 3$ °C, indicating that a major DNA-binding mode may be non-intercalative. This result agrees well with the evidence obtained from viscosity measurements and circular dichroism spectroscopy.

Noticeably, the ΔT_m values at the [complex]/[DNA] ratio = 2.0 are found to follow the trend of **2** > **4** > **1** > **3**, which correlates to their DNA-binding affinity.[62] In comparison with their starting compounds $[Cu(L^1)Cl_2]_2$ and $[Cu(L^2)Cl_2]_2$ (ΔT_m = 0.3–1.3 °C) under the same conditions,[12] higher ΔT_m values of **1–4** are observed. This may imply that all complexes in this system containing the N,N-heterocyclic ligands can bind to DNA more strongly than their initial compounds.

3.2.5. Quenching of DNA–ethidium bromide fluorescence by the copper(II) complexes. Fluorescence spectroscopy is a simple method which shows high sensitivity and selectivity. It is widely used to determine the interaction mode of DNA and the complexes. Ethidium bromide (EB) is a fluorescence indicator that can emit fluorescence when bound with DNA (EB–DNA complex) at 593 nm because of strong intercalative binding with adjacent DNA base pairs. The binding of another molecule to DNA can quench the emission intensity of EB, either by displacement of the EB and/or by accepting the exited state electron from EB through a photo-electron transfer mechanism.[63,64] The solutions of **1–4** in 3% MeOH/Tris-buffer at pH = 7.2 in the absence and presence of DNA show no fluorescence at room temperature. Upon addition of the complexes to the EB–DNA system with [complex]/[DNA] ratios of 0.1 to 1.0, all complexes can moderately decrease the intensity of EB–DNA complex (Fig. S8, ESI†), suggesting that the DNA-binding of all complexes probably occurs *via* (i) competing with EB at the same binding sites and/or (ii) interacting at different sites, as shown below.[65,66]

$$CuL + DNA\text{–}EB \rightleftharpoons DNA\text{–}CuL + EB \quad (i)$$

and/or

$$CuL + DNA\text{–}EB \rightleftharpoons EB\text{–}DNA\text{–}CuL \quad (ii)$$

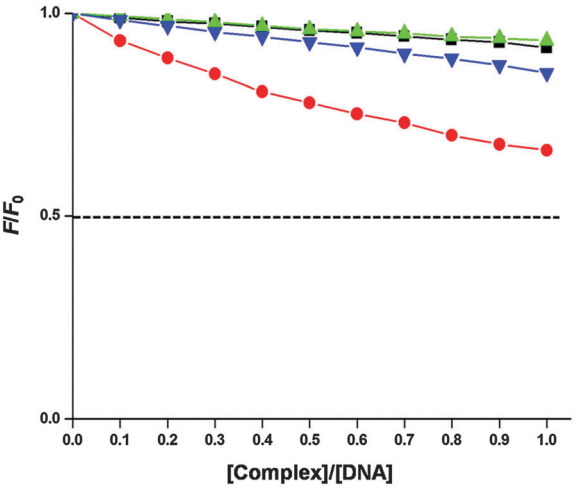

Fig. 6 Plots of the relative fluorescence quenching of EB–DNA complex treated by **1** (■), **2** (●), **3** (▲) and **4** (▼) at [complex]/[DNA] ratios of 0.1 to 1.0.

Principally, if a [complex]/[DNA] ratio < 100 is used and a quenching efficiency >50% is observed, the compound binds to DNA through an intercalative mode.[67] In this study, using [complex]/[DNA] ratios of 0.1 to 1.0, the EB–DNA emission intensities caused by the complexes decrease by less than 50% (Fig. 6), indicating that they may not interact with the double strand at the same sites as EB and may not replace EB. Hence, the complexes in this system possibly interfere with EB–DNA interaction and/or involve the formation of a non-fluorescence [EB–DNA–CuL] species, as described in pathway (ii). Moreover, the linearity of the Stern–Volmer plots (eqn (2)), as shown in the insets of Fig. S8 (ESI†), indicates that the quenching reaction is mainly carried out *via* a static quenching process[68] which involves the formation of a non-fluorescent species, as described in pathway (ii). Non-intercalation may be the major DNA-binding mode at low concentration. The quenching abilities of complexes **1–4**, evaluated by the Stern–Volmer quenching constant (K_{SV}), are in the order of **2** (1.07×10^4 M^{-1}) > **4** (3.24×10^3 M^{-1}) > **1** (1.76×10^3 M^{-1}) > **3** (1.49×10^3 M^{-1}), corresponding to their K_b values (see Table 3).

3.2.6. Determination of the DNA-binding stoichiometry of the copper(II) complexes. Determination of the DNA-binding stoichiometry of the copper(II) complexes is another method to further clarify their binding modes. The stoichiometric ratio is expressed by Cu (mmol)/DNA (mol base). These values can be analysed by considering the stoichiometric ratios of copper(II) aqua ion $[Cu(H_2O)_6]^{2+}$ (ratio > 150) and copper(II)–dipeptide complexes (ratio < 42).[22] If there is a large difference in the stoichiometry of the two compounds, it can be assumed that their DNA-interactions are dissimilar. The positively charged copper(II) aqua ion probably interacts with DNA by a less selective interaction, such as electrostatic attractions with the negatively charged phosphate groups. On the other hand, the significantly smaller stoichiometry of the copper(II)–dipeptide complexes suggests a more selective DNA-binding mode, such as intercalation. In this work, the obtained stoichiometry of **1–4** at a [complex]/[DNA] ratio of 1.0 exhibits 64, 77, 59 and

68 Cu (mmol)/DNA (mol base), respectively, which are slightly higher than that of the copper–dipeptide complexes. This result implies that the four compounds may bind to DNA *via* a non-intercalative mode under these conditions.

3.2.7. Possible DNA-binding modes. The results from the various efficient techniques described above are useful for the prediction of the possible DNA-binding interaction of complexes **1–4**. All evidence suggests that the four copper(II) complexes can interact with the DNA double helix *via* both non-intercalative and intercalative modes, depending on the [complex]/[DNA] ratio.

At a [complex]/[DNA] ratio < 1.0, the main DNA-binding behavior is expected to be non-intercalative. Upon increasing the amount of the complexes, their binding modes changed to intercalative interactions at [complex]/[DNA] ratios > 1.0 for **2** and **4**, > 1.5 for **1** and > 2.0 for **3**. This behavior may arise from the stability of the interactions between DNA and each complex. The changes in the binding modes of **2** and **4** from non-intercalation to intercalation occur at lower ratios than those of **1** and **3**. This supports the fact that the complexes containing 1,10-phenanthroline tend to bind to DNA *via* intercalation. In the case of **3**, its structure is the least planar; thus, it is difficult for this complex to interact with DNA through intercalation.

3.3. DNA cleavage studies of copper(II) complexes with pBR322 DNA

3.3.1. Gel electrophoresis. The DNA cleavage activities of the copper(II) complexes were investigated by determining the conversion of plasmid DNA, which is mainly in the supercoiled form (Form I), to the nicked circular (Form II) and linear forms (Form III) by electrophoresis. When electrophoresed, the three forms of DNA are separated by their different mobility rates on the gel. Relatively fast migration will be observed for Form I. Form II is the bulkiest; thus, it will move the slowest, while Form III will migrate between Forms I and II. The DNA cleavage activities of complexes **1–4** toward plasmid pBR322 DNA are shown in Fig. 7.

Upon increasing the complex concentration from 200 to 800 μM, increases in DNA Form II are observed in the electrophoretic bands. The complexes containing bipy (**1** and **3**) induce a slight increase in the band intensities of Form II, while the complexes containing phen (**2** and **4**) are considerably enhanced (Fig. S9, ESI†). However, all the complexes can partially cleave DNA Form I to Form II. The extent of the DNA cleavage potential at the final concentration of the complexes calculated by eqn (3) follows the order of **2** (57.70%) > **4** (50.70%) > **1** (31.60%) > **3** (9.37%).

Furthermore, the oxidative cleavage properties of the complexes were investigated by the addition of H_2ASC to mimic the reducing environment found inside the cells. The role of H_2ASC is to reduce Cu(II) to Cu(I), which then induces the formation of reactive oxygen species (ROS) that finally cleave the DNA. According to the different DNA-binding potentials of the four complexes, appropriate concentrations of the complexes are 10 to 400 μM for **1** and **3** and 0.1 to 4.0 μM for **2** and **4** in the presence of H_2ASC (100 μM), as demonstrated in Fig. 8.

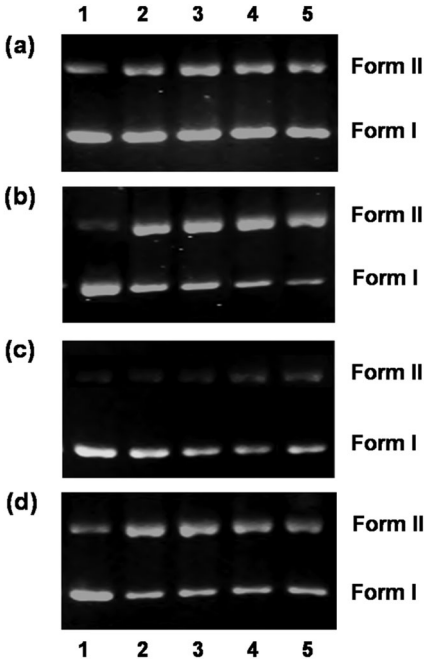

Fig. 7 Electrophoretic diagrams of supercoiled pBR322 DNA (0.2 μg, ~30 μM) cleaved by complexes (a) $[Cu(L^1)(bipy)]Cl_2$ (**1**); (b) $[Cu(L^1)(phen)]Cl_2$ (**2**); (c) $[Cu(L^2)(bipy)Cl_2]$ (**3**) and (d) $[Cu(L^2)(phen)]Cl_2$ (**4**) in HEPES-buffer. Incubation at 37 °C for 1 h. Lane 1, plasmid DNA alone; lanes 2 to 5, DNA + [complex] (200, 400, 600 and 800 μM, respectively).

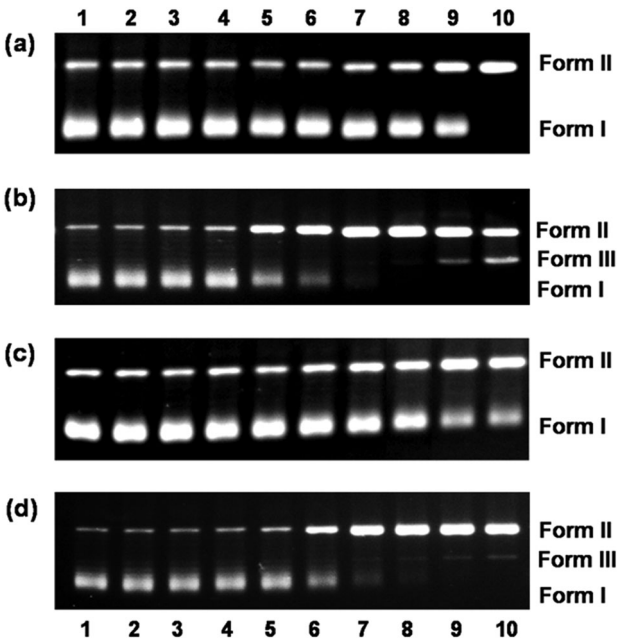

Fig. 8 Electrophoretic diagrams of supercoiled pBR322 DNA (0.2 μg, ~30 μM) cleaved by the complexes (a) $[Cu(L^1)(bipy)]Cl_2$ (**1**); (b) $[Cu(L^1)(phen)]Cl_2$ (**2**); (c) $[Cu(L^2)(bipy)Cl_2]$ (**3**) and (d) $[Cu(L^2)(phen)]Cl_2$ (**4**) in the presence of ascorbic acid (H_2ASC, 100 μM) in HEPES-buffer. Incubation at 37 °C for 1 h. Lane 1, plasmid DNA alone; lane 2, DNA + H_2ASC. For **1** and **3**: lanes 3 to 10, DNA + H_2ASC + [complex] (10, 20, 40, 60, 80, 100, 200 and 400 μM, respectively). For **2** and **4**: lanes 3 to 10, DNA + H_2ASC + [complex] (0.1, 0.2, 0.4, 0.6, 0.8, 1.0, 2.0 and 4.0 μM, respectively).

H_2ASC alone does not cause DNA cleavage (lane 2, Fig. 8). In the presence of **1** and **3**, Form II gradually increases from a concentration of 10 μM to 200 μM (lanes 3–9, Fig. 8a and c, respectively). At 400 μM (lane 10), complex **1** can totally cleave DNA Form I to Form II; however, complex **3** produces 52.77% of Form II (Fig. S10a and c, ESI†). In the case of **2** and **4**, both complexes significantly cleave Form I to Form II up to 1.0 μM; then Form II progressively increases to 2.0 μM (Fig. 8b and d). However, their DNA-cleavage potentials are different, as seen by the percentages of Form III of 31.1 and 6.55 in the presence of **2** and **4**, respectively (Fig. S10b and d, ESI†).

This behavior leads us to assume that the DNA cleavage behaviors of all the complexes in the presence of H_2ASC are possibly involved in the oxidative process by generating reactive oxygen species (ROS) such as hydrogen peroxide (H_2O_2), hydroxyl radical ($OH^\bullet$), singlet oxygen ($^1O_2$) or superoxide (O_2^-), which can cleave DNA.[69] The major role of these copper(II) complexes is based on the enzymatic properties of copper, which is important to the proposed mechanism of the *in situ* formation of H_2O_2, as shown below.[70,71]

$$H_2ASC + H_2O \rightleftharpoons HASC^- + H_3O^+ \quad \text{(iii)}$$

$$HASC^- + 2Cu(II) \rightarrow ASC + 2Cu(I) + H^+ \quad \text{(iv)}$$

$$2Cu(I) + O_2 + 2H^+ \rightarrow 2Cu(II) + H_2O_2 \quad \text{(v)}$$

$$HASC^- + O_2 + H^+ \rightarrow ASC + H_2O_2 \quad \text{(vi)}$$

Finally, hydrogen peroxide reacts with another equivalent of Cu(I) through the Fenton reaction (vii), producing a highly reactive species, hydroxyl radical, which is responsible for DNA oxidative damage.[70] This situation can be found for other copper(II) complexes whose DNA cleavage properties are increased by adding reducing agents, such as ascorbic acid.[12,72–74]

$$Cu(I) + H_2O_2 \rightarrow Cu(II) + OH^- + OH^\bullet \quad \text{(vii)}$$

In summary, all four complexes in this work can produce DNA strand scission in the presence of H_2ASC *via* the oxidative pathway; the order of efficiency is **2** > **4** > **1** > **3**, corresponding to their DNA-binding affinities.

3.3.2. Effect of the complexes on DNA morphology. Additional investigation into the interactions of the copper(II) complexes with DNA can be clearly visualized by atomic-force microscopy (AFM). The morphology changes of the plasmid pBR322 DNA induced by the complexes can be observed in the AFM images. The appropriate conditions utilized to obtain the AFM images of each complex are different, depending on their DNA cleavage reactivity. According to the electrophoretic experiments, plasmid DNA treated with the complexes in the presence of H_2ASC (100 μM) in HEPES-buffer was carried out under two conditions to acquire the AFM images (Fig. 9a–f): (i) 400 μM for **1** and **3** and (ii) 4 μM for **2** and **4**. After incubation, the supercoiled DNA alone (Form I) is not affected by H_2ASC (Fig. 9b). When treated with complex **1**, the supercoiled DNA is perfectly converted to the open circular DNA (Fig. 9c), while complex **3** shows partial DNA cleavage (Fig. 9e). Linear DNA can be found in the AFM images following treatment with complexes **2** and **4**. Notably, complex **2** can effectively cut the DNA strands into smaller linear forms (Fig. 9d) than complex **4** (Fig. 9f). The results from the AFM images are consistent with those obtained from the electrophoresis method (see lane 10 in Fig. 8).

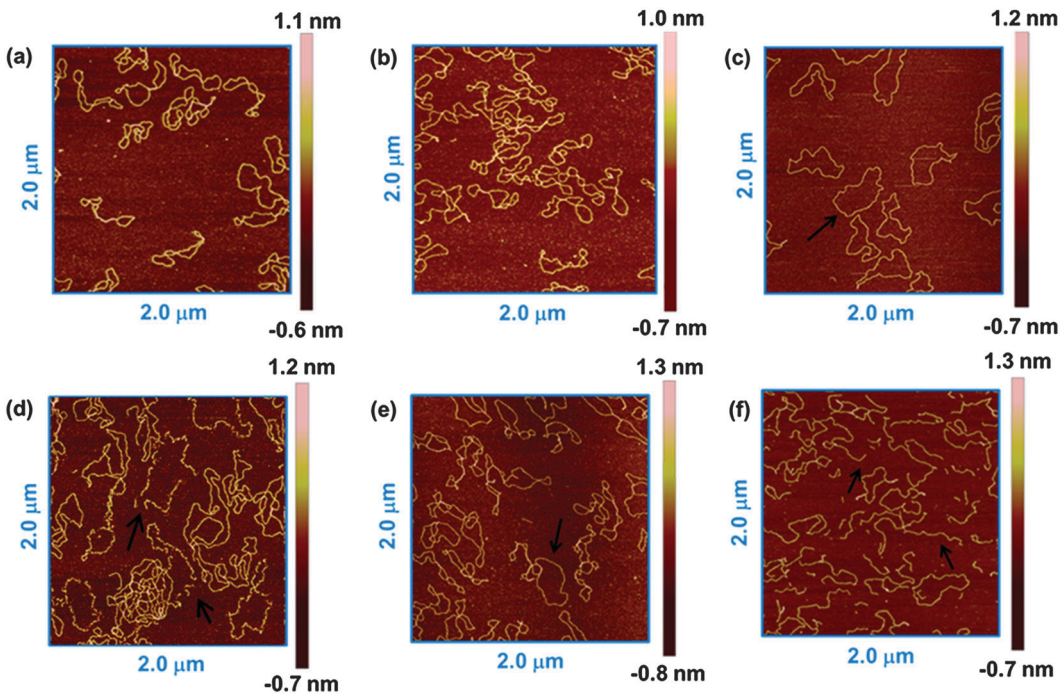

Fig. 9 AFM images showing the cleavage of supercoiled pBR322 DNA (0.2 μg) by copper(II) complexes with ascorbic acid (H_2ASC, 100 μM) in HEPES-buffer. Incubation at 37 °C for 1 h. (a) DNA alone; (b) DNA + H_2ASC; (c) DNA + H_2ASC + **1** (400 μM); (d) DNA + H_2ASC + **2** (4.0 μM); (e) DNA + H_2ASC + **3** (400 μM) and (f) DNA + H_2ASC + **4** (4.0 μM). Arrows indicate the obtained DNA morphologies after adding the copper(II) complexes and H_2ASC.

3.4. Anticancer activity of the copper(II) complexes

The four complexes **1–4** were further examined for their *in vitro* cytotoxicity against three human cancer cell lines, including small cell lung carcinoma (NCI-H187), oral cavity carcinoma (KB) and breast adenocarcinoma (MCF-7), by the resazurin microplate assay. Their anticancer activities are summarized in Table 6.

The obtained results revealed that the complexes in the present work have the potential to inhibit growth of the tested cancer cells but have different cytotoxic activities. However, complex **3** is active only toward NCI-H187 cells. According to their IC_{50} values, the degree of the anticancer activity of the complexes is in the order of **2** > **4** > **1** > **3**. It is noted that compounds **2** and **4**, which contain the phenanthroline ligand, show higher activity than compounds **1** and **3**, which contain the bipyridine ligand. These observations are in agreement with their potential DNA-binding and cleaving properties. Compared with the starting complexes $[Cu(L^1)Cl_2]_2$ and $[Cu(L^2)Cl_2]_2$, the complexes containing the additional N,N-heterocyclic ligands exhibit significantly greater activities (Table 6). Further comparisons are made with free N,N-heterocyclic molecules (bipy and phen) and cisplatin under the same conditions as **1–4**. Compound **1** is considerably more active against the KB and MCF-7 cell lines, but has lower activity against the NCI-H187 cell line than the free bipy. Meanwhile, compound **3** has lower cytotoxicity than the free bipy, which may arise from its structural features. In the case of phen, both **2** and **4** show dramatically better anticancer activity than the free phen. This behavior suggests that phen together with L^1 or L^2 in the compounds helps to improve the cytotoxic potential. Moreover, the cytotoxic properties of all complexes, except for **3**, are considerably greater than those of cisplatin. Complex **3** displays much lower cytotoxicity than the remaining three compounds. This may be due to the fact that it adopts a different geometry (octahedron) from the others (square planar). This result indicates that the factors controlling the anticancer activity are not only the type of ligand but also the coordination geometry.

3.5. Antibacterial activity studies

Previous reports revealed the interesting antibacterial activities of some copper(II) complexes of amidino-*O*-alkylurea derivatives against Bacillus,[75] *E. coli*,[12,76,77] *K. Pneumonia* and *P. mirabilis*,[76] *Salmonella* and *Campylobacter*.[10,12,77] Herein, our compounds containing amidino-*O*-methylurea derivatives and N,N-heterocycles were further tested to determine their *in vitro* antibacterial properties against *E. coli*, *Salmonella* and *Campylobacter* by the disc diffusion method. Their antibacterial activities were evaluated by their minimum inhibitory concentrations (MICs) (Table 7).

Table 6 Anticancer activities of **1–4** and the related compounds towards three human cancer cell lines

Complex	IC_{50} (μg mL^{-1})		
	KB	MCF-7	NCI-H187
$[Cu(L^1)Cl_2]_2$[a]	Inactive	Inactive	49.42
$[Cu(L^2)Cl_2]_2$[a]	22.51	Inactive	47.63
$[Cu(L^1)(bipy)]Cl_2$ (**1**)	17.97	6.61	24.23
$[Cu(L^1)(phen)]Cl_2$ (**2**)	1.08	0.97	1.07
$[Cu(L^2)(bipy)Cl_2]$ (**3**)	Inactive	Inactive	39.53
$[Cu(L^2)(phen)]Cl_2$ (**4**)	5.10	3.00	5.01
2,2′-Bipyridine	Inactive	Inactive	13.16
1,10-Phenanthroline	28.50	40.04	7.93
Cisplatin	27.01	Inactive	Inactive

[a] The starting complexes.

Table 7 Antibacterial activities of the complexes **1–4** and enrofloxacin against three human food-poisoning bacteria

Complex	MIC (mg mL^{-1})		
	E. coli	*Salmonella*	*Campylobacter*
$[Cu(L^1)Cl_2]_2$[a]	25.00	25.00	3.12
$[Cu(L^2)Cl_2]_2$[a]	25.00	12.50	3.12
$[Cu(L^1)(bipy)]Cl_2$ (**1**)	—	—	0.25
$[Cu(L^1)(phen)]Cl_2$ (**2**)	1.00	0.25	0.063
$[Cu(L^2)(bipy)Cl_2]$ (**3**)	—	—	—
$[Cu(L^2)(phen)]Cl_2$ (**4**)	1.00	1.00	0.125
Enrofloxacin	0.008	0.002	0.015

[a] The starting complexes.

Compound **2** is found to have the highest antibacterial activity toward the tested bacteria. Compound **4** also can inhibit the growth of all three bacteria, but has lower activity than **2**. Compound **1** is only active against *Campylobacter*. On the other hand, compound **3** gives the lowest potential, with no antibacterial activity toward all tested bacteria. Although their starting compounds can inhibit the growth of the three bacteria, they display considerably higher MIC values than **1** (for *Campylobacter*), **2** and **4**. This evidence strongly confirms that the existence of the N,N-heterocyclic ligand, particularly phen, together with L^1 or L^2 can improve the antibacterial activities of the complexes. However, compound **3** is inactive toward all tested pathogenic bacteria. This may arise from its proposed distorted octahedron structural geometry, which may not readily interact with the cells. This behavior is perfectly consistent with the DNA interaction potential of the complexes as well as their cytotoxicity.

Enrofloxacin, a well-known antibacterial drug, was also tested as a reference to compare with the complexes in this system. As expected, it exhibits much higher activity against the three tested bacteria. Although our compounds have less antibacterial potential than enrofloxacin, they still reveal greater inhibitory effects than their starting compounds. Therefore, it is promising to develop copper(II) compounds based on amidino-*O*-methylurea and its derivatives as antibacterial agents for a series of human-food poisoning bacteria in the future.

4. Conclusions

In this work, we have designed and synthesized four new copper complexes of amidino-*O*-methylurea (L^1) and *N*-(benzyl)-amidino-*O*-methylurea (L^2) containing the N,N-heterocyclic ligands (bipy and phen), $[Cu(L^1)(bipy)]Cl_2$ (**1**), $[Cu(L^1)(phen)]Cl_2$ (**2**), $[Cu(L^2)(bipy)Cl_2]$ (**3**) and $[Cu(L^2)(phen)]Cl_2$ (**4**). Compounds **1**, **2** and **4** are proposed to adopt a square planar CuN_4 geometry, while **3** is possibly a distorted octahedron. All complexes show DNA-binding properties, with two possible modes depending

on the concentration of the complex: non-intercalation at low concentration, and intercalation at high concentration. In addition, they exhibit DNA cleaving efficiency toward supercoiled DNA, possibly *via* an oxidative cleavage mechanism. Their anticancer activities toward small cell lung carcinoma (NCI-H187), oral cavity carcinoma (KB) and breast adenocarcinoma (MCF-7) cell lines is better than that of the starting complexes $[Cu(L^1)Cl_2]_2$ and $[Cu(L^2)Cl_2]_2$, particularly NCI-H187. Furthermore, the antibacterial activity against three gram negative bacteria (*E. coli*, *Salmonella* and *Campylobacter*) of **2** and **4** is considerably greater than that of **1** and **3**. The order of their DNA-binding and cleaving properties, as well as their anticancer and antibacterial potential, follows **2** > **4** > **1** > **3**. This result suggests that the complexes of ligand L^1 or L^2 with the planar phen display significantly higher cytotoxicity than the complexes containing bipy. This may arise from the fact that phen is more hydrophobic; hence, **2** and **4** diffuse more readily through the cancer and bacterial cell membranes.

In summary, the DNA-interacting properties and cytotoxicity of the complexes depend on the ligand type (L^1 or L^2), structural features and hydrophobicity. This complex system provides an interesting challenge of further study for development as a new generation agent for human cancer therapy and/or human food-poisoning treatment.

Acknowledgements

This work was financially supported by the Center of Excellence for Innovation in Chemistry (PERCH-CIC) and the Development and Promotion of Science and Technology Talents Projects (DPST) (to A. M.). We also thank the Higher Education Research Promotion and National Research University Project of Thailand, Office of the Higher Education Communication, through the Advanced Functional Materials Cluster of Khon Kaen University. P. G. acknowledges ICREA (Institució Catalana de Recerca i Estudis Avançats), the Ministerio de Economía y Competitividad of Spain (Project CTQ2011-27929-C02-01), and the support of COST Actions CM1003 and CM1105.

References

1 B. Rosenberg, L. van Camp, J. E. Trosko and V. H. Mansour, *Nature*, 1969, **222**, 385–386.
2 P. J. Loehrer and L. H. Einhorn, *Ann. Intern. Med.*, 1984, **100**, 704–713.
3 A. Eastman, Cisplatin, in *Chemistry and Biochemistry of a Leading Anticancer Drug*, ed. B. Lippert, VHCA & Wiley-VCH, Zurich & Germany, 1999, pp. 111–134.
4 J. R. R. Frausto da Silva and R. J. P. Williams, *The Biological Chemistry of the Element: Inorganic Chemistry of Life*, Clarendon Press, New York, 1991, pp. 40–41, 389–399.
5 T. Ma, J. Xu, Y. Wang, H. Yu, Y. Yang, Y. Liu, W. Ding, W. Zhu, R. Chen, Z. Ge, Y. Tan, L. Jia and T. Zhu, *J. Inorg. Biochem.*, 2015, **144**, 38–46.
6 P. P. Silva, W. Guerra, G. C. Santos, N. G. Fernandes, J. N. Silveira, A. M. C. Ferreira, T. Bortolotto, H. Terenzi, A. J. Bortoluzzi, A. Neves and E. C. Pereira-Mai, *J. Inorg. Biochem.*, 2014, **132**, 67–76.
7 N. Raman, R. Mahalakshmi and L. Mitu, *Spectrochim. Acta, Part A*, 2014, **131**, 355–364.
8 P. Hubberstey, U. Suksangpanya and C. Wilson, *CrystEngComm*, 2000, **26**, 141–145.
9 U. Suksangpanya, A. J. Blake, P. Hubberstey, D. J. Parker, S. J. Teat and C. L. Wilson, *CrystEngComm*, 2003, **5**, 10–22.
10 U. Chaveerach, A. Meenongwa, Y. Trongpanich, C. Soikum and P. Chaveerach, *Polyhedron*, 2010, **29**, 731–738.
11 M. J. Begley, P. Hubberstey and C. H. M. Moore, *J. Chem. Res.*, 1986, 172–173.
12 A. Meenongwa, R. F. Brissos, C. Soukum, P. Chaveerach, P. Gamez, Y. Trongpanich and U. Chaveerach, *New J. Chem.*, 2015, **39**, 664–675.
13 S. Iglesias, N. Alvarez, M. H. Torre, E. Kremer, J. Ellena, R. R. Ribeiro, R. P. Barroso, A. J. Costa-Filho, M. G. Kramer and G. Facchin, *J. Inorg. Biochem.*, 2014, **139**, 117–123.
14 A. Galani, E. K. Efthimiadou, G. Mitrikas, Y. Sanakis, V. Psycharis, C. Raptopoulou, G. Kordas and A. Karaliota, *Inorg. Chim. Acta*, 2014, **423**, 207–218.
15 J. D. C. Almeida, D. A. Paixão, I. M. Marzano, J. Ellena, M. Pivatto, N. P. Lopes, A. M. D. C. Ferreira, E. C. Pereira-Maia, S. Guilardi and W. Guerra, *Polyhedron*, 2015, **89**, 1–8.
16 A. Meenongwa, U. Chaveerach and K. Siriwong, *Inorg. Chim. Acta*, 2011, **366**, 357–365.
17 J. Marmur, *J. Mol. Biol.*, 1961, **3**, 208–218.
18 M. F. Reichmann, S. A. Rice, C. A. Thomas and P. Doty, *J. Am. Chem. Soc.*, 1954, **76**, 3047–3053.
19 A. Wolfe, G. H. Shimer and T. Meehan, *Biochemistry*, 1987, **26**, 6392–6396.
20 G. Cohen and H. Eisenberg, *Biopolymers*, 1969, **8**, 45–49.
21 J. R. Lakowicz and G. Weber, *Biochemistry*, 1973, **12**, 4161–4170.
22 G. Facchin, E. Kremer, D. A. Barrio, S. B. Etcheverry, A. J. Costa-Filho and M. H. Torre, *Polyhedron*, 2009, **28**, 2329–2334.
23 M. F. Shubsda, J. Goodisman and J. C. Dabrowiak, *J. Biochem. Biophys. Methods*, 1997, **34**, 73–79.
24 M. N. Patel, P. A. Dosi and B. S. Batt, *Polyhedron*, 2010, **29**, 3238–3245.
25 J. O. Brien, I. Wilson, T. Orton and F. Pognan, *Eur. J. Biochem.*, 2000, **267**, 5421–5426.
26 M. J. O'Neill, D. H. Bray, P. Boardmann, J. D. Phillipson and D. C. Warhurst, *Planta Med.*, 1985, **51**, 394–398.
27 C. H. Collins and P. M. Lyne, *Microbiological Methods*, University Park Press, Baltimore, 1970, p. 422.
28 E. J. L. Lana, F. Carazza and J. A. Takahashi, *J. Agric. Food Chem.*, 2006, **54**, 2053–2056.
29 R. S. Kumar, K. Sasikala and S. Arunachalam, *J. Inorg. Biochem.*, 2008, **102**, 234–241.
30 G. Marcon, S. Carotti, M. Coronnello, L. Messori, E. Mini, P. Orioli, T. Mazzei, M. A. Cinellu and G. Minghetti, *J. Med. Chem.*, 2002, **45**, 1672–1677.
31 R. A. Macleod, *J. Biol. Chem.*, 1952, **197**, 751–761.
32 C. Krishmanurti, L. A. Saryan and D. H. Petering, *Cancer Res.*, 1980, **40**, 4092–4099.

33 P. R. Reddy, A. Shilpa, N. Raju and P. Raghavaiah, *J. Inorg. Biochem.*, 2011, **105**, 1603–1612.
34 M. Satterfield and J. S. Brodbelt, *Inorg. Chem.*, 2001, **40**, 5393–5400.
35 J. Shen and J. Brodbelt, *J. Mass Spectrom.*, 1999, **34**, 137–146.
36 B. Louis, C. Detoni, N. M. F. Carvalho, C. D. Duarte and O. A. C. Antunes, *Appl. Catal., A*, 2009, **360**, 218–225.
37 R. Starosta, U. K. Komarnicka, M. Sobczyk and M. Barys, *J. Lumin.*, 2012, **132**, 1842–1847.
38 W. K. Musker and M. S. Hussain, *Inorg. Chem.*, 1969, **8**, 528–536.
39 B. J. Hathaway, *J. Chem. Soc., Dalton Trans.*, 1972, 1196–1199.
40 P. Comba, N. F. Curtis, G. A. Lawrance, A. M. Sargeson, B. W. Skelton and A. H. White, *Inorg. Chem.*, 1986, **25**, 4260–4267.
41 I. M. Proctor, B. J. Hathaway and P. Nichols, *J. Chem. Soc. A*, 1968, 1678–1684.
42 D. N. Zimmerman and J. L. Hall, *Inorg. Chem.*, 1973, **12**, 2616–2620.
43 B. J. Hathaway and D. E. Billing, *Coord. Chem. Rev.*, 1970, **5**, 143–207.
44 B. A. Goodman and J. B. Raynor, Electron spin resonance of transition metal complexes, in *Adv. Inorg. Chem. Radiochem.*, ed. H. J. Emeléus and A. G. Sharpe, Academic Press, New York, 1970, vol. 13, pp. 135–362.
45 G. Tabbi, A. Giuffrida and R. P. Bonomo, *J. Inorg. Biochem.*, 2013, **128**, 137–145.
46 J. R. Wasson and C. Trapp, *J. Phys. Chem.*, 1969, **73**, 3763–3772.
47 A. C. Mot, S. A. Syrbu, S. V. Makarov, G. Damian and R. Silaghi-Dumitrescu, *Inorg. Chem. Commun.*, 2012, **18**, 1–3.
48 G. M. Blackburn, M. J. Gait and D. Loakes, Reversible Small Molecule-Nucleic Acid Interactions, in *Nucleic acid in chemistry and biology*, ed. D. M. Williams, RSC Publishing, Cambridge, 3rd edn, 2006, pp. 342–382.
49 L. S. Lerman, *J. Mol. Biol.*, 1961, **3**, 18–30.
50 E. C. Long and J. K. Barton, *Acc. Chem. Res.*, 1990, **23**, 271–273.
51 R. F. Pasternack, E. J. Gibbs and J. Villafranca, *Biochemistry*, 1983, **22**, 2406–2414.
52 G. Pratviel, J. Bernadou and B. Meunier, *Adv. Inorg. Chem.*, 1998, **45**, 251–312.
53 Q. Li, P. Yang, H. Wang and M. Guo, *J. Inorg. Biochem.*, 1996, **64**, 181–195.
54 J. B. Lambert, H. F. Shurvell, L. Verbit, R. G. Cooks and G. H. Stout, *Organic structural analysis*, Macmillan Publishing, New York, 1976.
55 S. P. Devi, R. K. B. Devi, M. Damayanti, N. R. Singh and R. K. H. Singh, *Polyhedron*, 2012, **47**, 1–8.
56 Z. S. Yang, Y. L. Wang and G. C. Zhao, *Anal. Sci.*, 2004, **20**, 1127–1130.
57 T. Gupta, S. Dhar, M. Nethaj and A. R. Chakravaty, *Dalton Trans.*, 2004, 1896–1900.
58 J. Z. Wu, B. H. Ye, L. Wang, L. N. Ji, J. Y. Zhou, R. H. Li and Z. Y. Zhou, *J. Chem. Soc., Dalton Trans.*, 1997, 1395–1401.
59 S. Satyanarayana, J. C. Dabrowiak and J. B. Chaires, *Biochemistry*, 1992, **31**, 9319–9324.
60 D. S. Raja, N. S. P. Bhuvanesh and K. Natarajan, *Inorg. Chim. Acta*, 2012, **385**, 81–93.
61 V. I. Ivanov, L. E. Minchenkova, A. K. Schyolkina and A. I. Poletayev, *Biopolymers*, 1973, **12**, 89–110.
62 G. A. Neyhart, N. Grover, S. R. Smith, W. Kalsbeck, T. A. Fairley, M. Cory and H. H. Thorp, *J. Am. Chem. Soc.*, 1993, **115**, 4423–4428.
63 B. C. Baguley and M. LeBret, *Biochemistry*, 1984, **23**, 937–943.
64 R. F. Pasternack, M. Cacca, B. Keogh, T. A. Stephenson, A. P. Williams and F. J. Gibbs, *J. Am. Chem. Soc.*, 1991, **113**, 6835–6840.
65 E. Nyarko, N. Hanada, A. Habib and M. Tabata, *Inorg. Chim. Acta*, 2004, **357**, 739–745.
66 V. C. Silveira, H. Benezra, J. S. Luz, R. C. Georg, C. C. Oliveira and A. M. C. Ferreira, *J. Inorg. Biochem.*, 2011, **105**, 1692–1703.
67 X. Ling, W. Zhong, Q. Huang and K. Ni, *J. Photochem. Photobiol., B*, 2008, **93**, 172–176.
68 J. R. Lakowicz, *Principles of Fluorescence Spectroscopy*, Plenum Press, New York, 3rd edn, 2006, pp. 277–286.
69 B. Halliwell and J. M. C. Gutteridge, *Free Radicals in Biology and Medicine*, Oxford Science Publication, Oxford, 3rd edn, 1999, pp. 42–43.
70 D. S. Sigman and C. H. B. Chen, *Acc. Chem. Res.*, 1986, **19**, 180–186.
71 I. Yamazaki and L. H. Piette, *Biochim. Biophys. Acta*, 1961, **59**, 62–69.
72 M. Ganeshpandian, R. Loganathan, S. Ramakrishnan, A. Riyasdeen, M. A. Akbarsha and M. Palaniandavar, *Polyhedron*, 2013, **52**, 924–938.
73 X. B. Fu, G. T. Weng, D. D. Liu and X. Y. Le, *J. Photochem. Photobiol., A*, 2014, **276**, 83–95.
74 X. B. Fu, J. J. Zhange, D. D. Liu, Q. Gan, H. W. Gao, Z. W. Mao and X. Y. Le, *J. Inorg. Biochem.*, 2015, **143**, 77–87.
75 O. I. Singh, M. Damayanti, N. R. Singh, R. K. H. Singh, M. Mohapatra and R. M. Kadam, *Polyhedron*, 2005, **24**, 909–916.
76 S. P. Devi, R. K. B. Devi, M. Damayanti, N. R. Singh, R. K. H. Singh and R. M. Kadam, *J. Coord. Chem.*, 2011, **64**, 1586–1601.
77 R. Pretumwieng, C. Soikum, P. Chaveerach and U. Chaveerach, *Inorg. Chim. Acta*, 2014, **423**, 421–429.

